

HA-VLN: A Benchmark for Human-Aware Navigation in Discrete–Continuous Environments with Dynamic Multi-Human Interactions, Real-World Validation, and an Open Leaderboard

Yifei Dong^{1*} Fengyi Wu^{1*} Qi He^{1*} Heng Li¹ Minghan Li² Zebang Cheng¹
 Yuxuan Zhou³ Jingdong Sun⁴ Qi Dai⁵ Zhi-Qi Cheng^{1†} Alexander G. Hauptmann⁴

¹University of Washington ²Galbot ³University of Mannheim

⁴Carnegie Mellon University ⁵Microsoft Research

Abstract

*Vision-and-Language Navigation (VLN) systems often focus on either discrete (panoramic) or continuous (free-motion) paradigms alone, overlooking the complexities of human-populated, dynamic environments. We introduce a unified Human-Aware VLN (HA-VLN) benchmark that merges these paradigms under explicit social-awareness constraints. Our contributions include: (1) a standardized task definition that balances discrete–continuous navigation with personal-space requirements; (2) an enhanced human motion dataset (HAPS 2.0) and upgraded simulators capturing realistic multi-human interactions, outdoor contexts, and refined motion–language alignment; (3) extensive benchmarking on 16,844 human-centric instructions, revealing how multi-human dynamics and partial observability pose substantial challenges for leading VLN agents; (4) real-world robot tests validating sim-to-real transfer in crowded indoor spaces; and (5) a public leaderboard supporting transparent comparisons across discrete and continuous tasks. Empirical results show improved navigation success and fewer collisions when social context is integrated, underscoring the need for human-centric design. By releasing all datasets, simulators, agent code, and evaluation tools, we aim to advance safer, more capable, and socially responsible VLN research.**

1. Introduction

Vision-and-Language Navigation (VLN) [3, 56] enables robots to understand multimodal instructions and navigate real or simulated spaces [15, 49]. While recent VLN systems have shown encouraging results in constrained domains, most focus exclusively on either *discrete*

(panoramic) or *continuous* (free-motion) navigation, omitting the rich human dynamics and partial observability of realistic environments [4, 23, 54]. These omissions compromise real-world applicability, as embodied agents must handle unpredictable human motion, avoid collisions, and process instructions referencing socially salient cues.

Motivation & Gaps. Despite notable progress, three major challenges persist in today’s VLN research. *First, social awareness* remains underexplored: human participants in the scene are commonly overlooked or reduced to inert obstacles, preventing the agent from respecting personal space or reacting to bystanders’ activities (see Figure 1). *Second, instruction complexity* is not well captured in existing corpora [39]. Commands such as “*Turn to your left, and go past the chair*” rarely reflect real-world contexts like “*Turn to your left, where you will see someone taking a brief pause ... on the chair*” in Figure 1. *Third, static-environment assumptions* dominate, neglecting real-time re-planning when people traverse corridors or gather spontaneously. In practice, social navigation demands partial observability and dynamic route adjustment.

Human-Aware VLN. To tackle these limitations, Human-Aware VLN (HA-VLN) [31] explicitly integrates *dynamic human interactions*, driving agents to navigate among people engaged in various everyday behaviors. Although HA-VLN moves closer to realistic settings, it remains constrained by four main issues (Appendix Table A1): (1) *Limited Human Motion Data*, as initial datasets (e.g., HAPS 1.0 [31]) sometimes misalign textual labels and 3D motion sequences; (2) *Discrete Navigation Bias*, since many simulators restrict navigation to panoramic hops [28]; (3) *Underdeveloped Multi-Human Interactions*, typically modeling only a single person in indoor scenes; and (4) *Instruction Generation Deficits*, where automated text expansions omit time-varying human behaviors, limiting agents’ adaptability in dynamic, crowded environments.

Our Approach & Contributions. In this paper, we sub-

*Equal contribution. Work done during internship at UW.

†Corresponding author.

*Project: <https://ha-vln-project.vercel.app/>

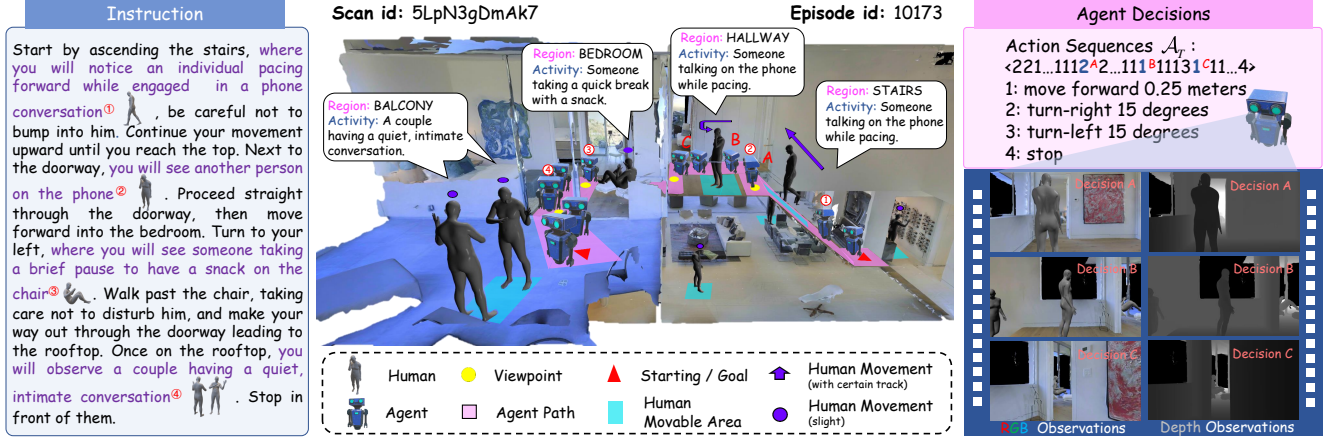


Figure 1. **HA-VLN Navigation Scenario.** An agent navigates environments with dynamic human activities, adjusting its path based on natural language instructions and real-time sensor observations to avoid collisions. Key positions (e.g., ①, ②) align with *instructional cues* referring to specific human behaviors. When the agent encounters a bystander on the phone (②, Decision A), it intelligently turns right to avert a potential collision. On the right, RGB and Depth observations illustrate the agent’s panoramic view preceding decisions A, B, and C, capturing its dynamic responses to nearby humans. [Best viewed in color and high resolution.]

stantially extend HA-VLN by unifying discrete and continuous navigation, coupling high-fidelity human motion data, multi-agent interactions, and real-time rendering under a single umbrella. Concretely, we make four primary contributions, each elaborated in its respective section:

- **Standardized Task & Metrics [Sec. 2].** We unify discrete and continuous navigation under social-awareness constraints, ensuring consistent goals and evaluations.
- **Upgraded Data & HA-VLN Simulator [Sec. 3].** Building on HAPS 1.0 [31], we present HAPS 2.0 (486 SMPL sequences) and two advanced simulators (HA-VLN-DE, HA-VLN-CE) that incorporate multi-view human annotation, dual-thread rendering, and rigorous collision checks for up to 910 active individuals (Figure 2).
- **Comprehensive Benchmarking [Sec. 4].** We enrich R2R-CE with 16,844 human-centric instructions (Table A3) and benchmark multiple agents under unified metrics, unveiling challenges arising from multi-human dynamics and partial observability.
- **Real-World Validation & Leaderboard [Sec. 5].** We robustly demonstrate sim-to-real transfer using a physical robot successfully navigating crowded indoor areas, and provide a public leaderboard for comprehensive discrete-continuous evaluations in multi-human scenarios.

As visualized in Figures 1 and 2, introducing realistic human motion significantly amplifies task complexity, leading to pronounced performance drops in baseline VLN models. By bridging discrete and continuous navigation, enriching human-motion fidelity, and validating results both in simulation and on physical robots, our approach narrows the gap between conventional VLN setups and real-world, socially aware navigation systems. We release all related datasets, simulators, agent code, and evaluation tools to further fuel

progress in this emerging research area.

2. Human-Aware VLN Task

Motivation & Overview. We present *Human-Aware Vision-and-Language Navigation* (HA-VLN), a next-generation VLN framework that specifically requires agents to navigate among dynamically moving people while following natural-language instructions. Unlike standard VLN—where humans are either absent or treated as static obstacles—HA-VLN compels agents to anticipate human motion, respect personal space, and adapt paths to avoid collisions. As shown in Figure 1, the agent must interpret instructions referencing ongoing activities (e.g., “*Go upstairs where someone is pacing on the phone...*”) and then maneuver accordingly in a photorealistic 3D space.

State & Action Spaces. At each time step t , the agent’s state is

$$s_t = \langle \mathbf{p}_t, o_t, \Theta_t^{\text{FOV}} \rangle,$$

where \mathbf{p}_t is its 3D location, o_t its orientation, and Θ_t^{FOV} its egocentric view. In **discrete environments (DE)**, agents hop among pre-defined viewpoints, each providing an RGB observation. In **continuous environments (CE)**, agents see an RGB+D feed with a 90° field of view and can move in small increments (e.g., 0.25 m forward, 15° turn). Across both settings, the action space is

$$\mathcal{A} = \{a_{\text{forward}}, a_{\text{left}}, a_{\text{right}}, a_{\text{up}}, a_{\text{down}}, a_{\text{stop}}\}.$$

Figure 2 provides examples of how these actions evolve within complex, human-occupied scenes.

Human-Aware Constraints. Beyond reaching a goal, agents must obey strict social protocols:

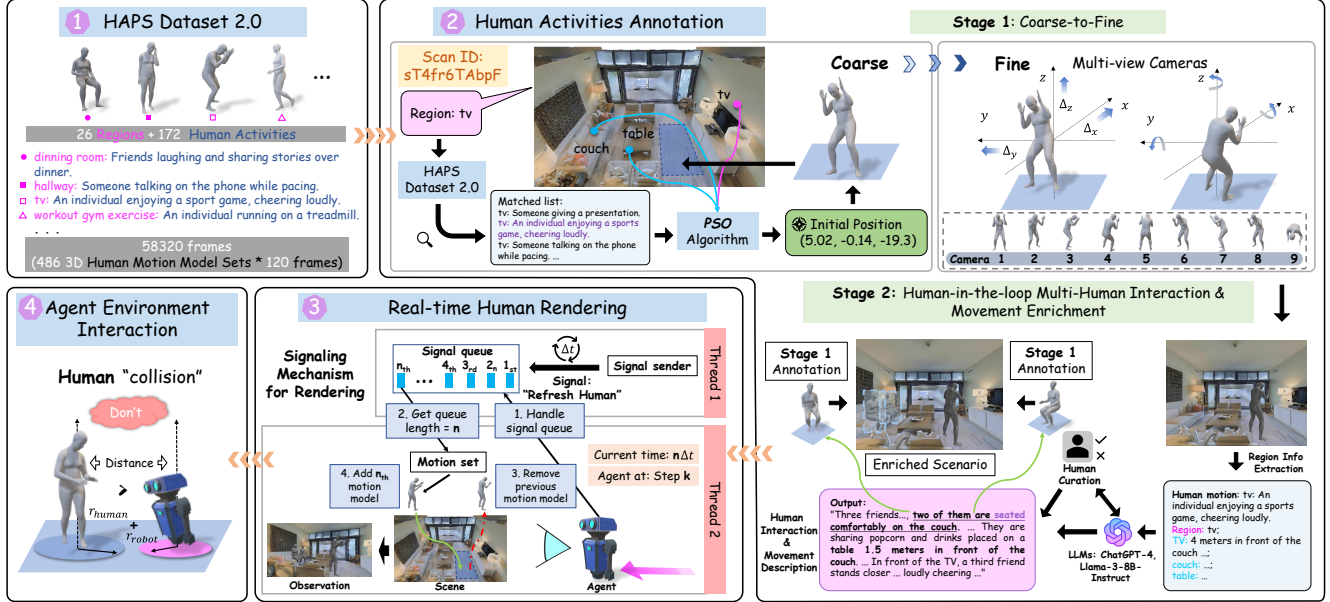


Figure 2. **HA-VLN-CE Simulator.** We extend photorealistic Habitat environments by integrating diverse and dynamic human activities using the HAPS 2.0 dataset (172 activities, 486 motion models, 58,320 frames). The annotation pipeline proceeds in two stages: (i) a *coarse-to-fine* optimization approach with PSO and synchronized multi-view cameras, and (ii) a *human-in-the-loop* iterative refinement process to enrich multi-human interactions and movements. Real-time rendering uses a signaling mechanism to update human motion dynamically, enabling continuous collision detection and agent-environment interplay. [Best viewed in color and high resolution.]

- **Dynamic Human Models.** People move naturally according to 3D motion trajectories from HAPS 2.0, which are continuously updated in real time.
- **Personal Space.** Agents must avoid getting too close (under 3 m in DE or within the sum of radii in CE).
- **Human-Focused Instructions.** Language often describes people and their activities (e.g., “Go around the person talking on the phone”), necessitating alignment between textual prompts and live visual inputs.

These detailed human placements and movements are annotated via a multi-stage pipeline (Sec. 3), entailing extensive labeling and verification to ensure realism.

Dynamic & Partial Observations. Because people can move unpredictably, each time step is a partially observable Markov decision process (POMDP). The new state s_{t+1} depends on both the agent’s action and concurrent human movements (e.g., someone stepping aside or emerging from a corridor). Agents must infer unobserved factors—such as whether a person will yield space—and balance *exploration* (seeking alternative routes) and *exploitation* (continuing on a known path) to reach the target efficiently.

Challenges & DE-CE Synergies. Building socially compliant robots in crowded settings poses three key Sim2Real challenges: (i) *Social Navigation*, i.e., collision-free motion that respects personal space; (ii) *Human-Aligned Instructions*, where language may refer to fleeting activities or interactions; and (iii) *Adaptive Re-Planning*, as humans can block or unblock hallways unpredictably. While **DE**

allows rapid prototyping via discrete viewpoint jumps, **CE** approximates real-world dynamics and motion fidelity. By integrating both approaches, HA-VLN spans the spectrum from large-scale simulation to practical on-robot deployment, significantly broadening research in socially aware, human-centric navigation.

3. HA-VLN Simulator

Motivation & Overview. The *HA-VLN Simulator* addresses long-standing challenges in socially-aware navigation by placing multiple, dynamically moving humans into both *discrete* and *continuous* 3D environments. While many existing simulators either overlook human behaviors or model them as static obstacles, our simulator features high-fidelity motion, multi-person interactions, and real-world complexities such as group gatherings, spontaneous movements, and personal-space constraints. Table A2 situates our approach relative to *Habitat 3.0* [42] and *Habi-Crowd* [48], highlighting broader scenario coverage, more natural motion types, and explicit instruction alignment. Meanwhile, Table A3 contrasts *HAPS 2.0* with its predecessor, *HAPS 1.0* [31], underscoring notable advancements in motion diversity, alignment accuracy, and overall realism. By building on HAPS 2.0, we leverage 486 motion sequences that span indoor and outdoor activities. We provide two complementary modules: **HA-VLN-CE** for continuous navigation and **HA-VLN-DE** for discrete navigation. Both

modules share a unified API (Sec. 3), offering consistent access to human states, dynamic scene updates, and collision checks. Figure 2 presents an overview of how these elements converge within an agent’s action-observation loop.

HAPS 2.0 Dataset. Evolving from *HAPS 1.0* [31], HAPS 2.0 encompasses 486 3D human-activity descriptions covering 26 region types (e.g., living rooms, gyms, sidewalks). Each description (e.g., “workout gym exercise: An individual running on a treadmill”) is validated through human surveys and ChatGPT-4 [6] for plausibility. We employ the Motion Diffusion Model (MDM) [17] to transform these text descriptions into 120-frame SMPL mesh sequences, $\mathcal{H} = \langle h_1, \dots, h_{120} \rangle$, capturing detailed 3D pose and shape information. Figure A2 illustrates various indoor and outdoor contexts, while Figure A3 depicts representative motions (e.g., climbing stairs, running).

Annotation Pipeline: Coarse-to-Fine. To position these motions in large-scale 3D scans, we employ a two-stage annotation procedure. *Stage 1 (Coarse)* uses Particle Swarm Optimization (PSO) [25] (Algorithm A1) to allocate motions within each region \mathbf{R} , bounded by $\mathbf{B}_{lo}, \mathbf{B}_{hi}$, and link them to suitable objects \mathbf{O} . A subset $\mathbf{H}' \subseteq \mathbf{H}$ is filtered by region labels, then paired with objects via semantic cues (e.g., “sitting on a chair” aligns with a *chair* object). PSO penalizes boundary violations and personal-space intrusions (1 m), producing highly plausible initial placements. *Stage 2 (Fine)* refines these placements with a precise nine-camera approach [22, 40] (Figure A1). Annotators iteratively adjust rotations and positions to eliminate collisions or interpenetrations (e.g., limbs intersecting walls), requiring over 430 hours of human labeling to achieve 529 precisely aligned models across 90 scans. To further enhance diversity, we integrate a human-in-the-loop process [11] for generating multi-person scenarios: large language models propose contextual interactions (Listings 1 and 2), which annotators then refine. Figure A3 illustrates enhanced interactions (e.g., group discussions). After both stages, we assemble 910 human models distributed over 428 regions in 90 scans, including 268 complex motions (e.g., running, stair climbing). Figure A5 and Appendix B.8 detail their distributions, revealing extensive coverage of diverse motion types and scene layouts.

Real-Time Rendering & Agent Interaction. Our simulator updates human motions in real time rather than relying on static captures. A dual-thread producer-consumer architecture (Algorithm A2) orchestrates frame updates, with Thread 1 enqueueing “refresh” signals and Thread 2 processing them in sync with the agent’s action cycle. Each motion spans up to 120 frames; once Thread 2 detects a signal, it discards old meshes and loads new ones, maintaining retrieval delays under 50 ms. Figure A2 exemplifies how multiple humans can simultaneously populate a shared environment. Agents perceive these moving entities through

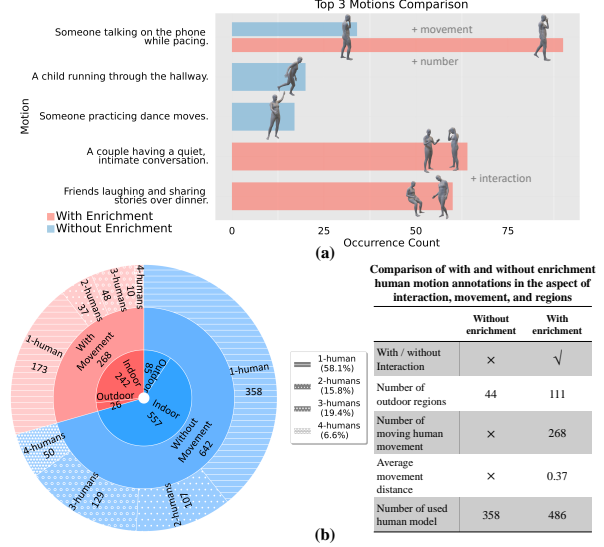


Figure 3. Motion Analysis. (a) Top three motions from Stage 1 (*without* enrichment) and Stage 2 (*with* enrichment). (b) Overall statistics of human activities, comparing interaction types, movement distances, and the number of models used. Enrichment extends both the variety and dynamic aspects of human activities.

a navigation mesh (navmesh) [45]. Collisions are flagged if the distance between bounding volumes is less than their combined radii, leading to an automatic revert. This mechanism ensures agents learn to respect personal space and navigate effectively around dynamic crowds.

Discrete vs. Continuous Settings. HA-VLN-CE (Continuous) allows agents to move in real-valued increments (e.g., 0.25 m forward, 15° turns), supporting fine-grained collision avoidance and social reactivity. As Figure A5 shows, each scene can contain up to 10 humans, with simulation speeds reaching 30–60 FPS on standard GPUs. **HA-VLN-DE** (Discrete) extends *HA3D* [31] to incorporate HAPS 2.0 data, encompassing both indoor and outdoor settings. Here, agents hop among panoramic viewpoints while humans continue to move, preserving core social-navigation challenges. We map continuous positions to discrete viewpoints [31], add small offsets to refine alignment, and integrate 627 annotated humans across 90 buildings.

Unified API. We provide a unified API for both modes with three core functionalities: (1) *Human State Queries* retrieve bounding volumes, motion frames, and semantic annotations of nearby humans; (2) *Dynamic Scene Updates* notify agents of newly moved humans or environmental changes; and (3) *Collision Checks* detect whether a proposed move (e.g., forward step or viewpoint hop) would result in intersection with a human. By unifying HAPS 2.0 with coarse-to-fine annotation, real-time multi-human rendering, and a single API across discrete and continuous settings, our *HA-VLN Simulator* significantly broadens the scope of socially-aware navigation research. Figures A2, A3, and A5 de-

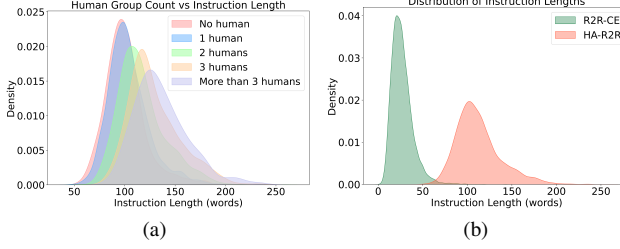


Figure 4. **HA-R2R Dataset Analysis.** (a) Instruction-length distribution by human group size (no humans to more than three). (b) Comparison of instruction lengths between HA-R2R and R2R-CE.

pict the simulator’s capacity to capture rich human behaviors, while Tables A1 and A3 underscore our advantages over earlier simulators, including Habitat 3.0 and Habi-Crowd, as well as the improvements of HAPS 2.0 relative to HAPS 1.0. Appendix B.7 outlines environment sizes, latency considerations, and usage examples.

4. HA-VLN Agents

This section introduces our **Human-Aware Room-to-Room (HA-R2R)** dataset and two navigation agents: **HA-VLN-VL** and **HA-VLN-CMA**. We aim to endow agents with enhanced understanding of social cues—respecting personal space, avoiding collisions, and reacting to bystanders. As illustrated in Figures A8 and A9, dynamic human behaviors impose additional complexity and variability, necessitating robust perception and policy strategies.

HA-R2R Dataset. Although the Room-to-Room in Continuous Environment (**R2R-CE**) dataset [28] supports continuous navigation, it lacks explicit focus on human interactions. We therefore develop **HA-R2R**, which extends R2R-CE with 16,844 carefully curated instructions highlighting social nuances (e.g., conversations, corridor crossings, near-collision events). Table A4 showcases representative directives, while Figure A6 reveals the expanded vocabulary centered around human-centric language.

To generate these enriched instructions, we design targeted prompts for large language models (Appendix C.2), capturing a diverse range of real-world social scenarios. This augmentation marks a significant leap from static paths to ones requiring agents to interpret, for example, “avoid the couple chatting near the bar” or “yield to someone crossing the hallway.” Our comparative analysis between baseline and augmented instructions (Appendix C.3) highlights both the extensive annotation workload and the potential of HA-R2R to advance *human-aware* navigation research.

HA-VLN-VL Agent. HA-VLN-VL agent focuses on *visual-language alignment* when encountering socially enriched instructions. Adapted from Recurrent VLN-BERT [20], it discards actor-critic methods (e.g., A2C [27]) in favor of a simpler *imitation learning* approach, thereby emphasizing how stronger multimodal grounding alone can elevate performance in complex settings.

Algorithm 1 HA-VLN-CMA Training Procedure

Require: Expert policy π^* , parameters θ , replay buffer B
Ensure: Trained CMA model parameters θ

- 1: Initialize parameters θ (e.g., via imitation learning)
- 2: **for** iteration = 1 **to** N **do**
- 3: Execute policy π_θ to collect rollouts
- 4: With probability β , follow expert π^*
- 5: Store (s_t, a_t, r_t) in B
- 6: Apply Envdrop to (v_t, l)
- 7: $\theta \leftarrow \theta - \eta \nabla_\theta \mathcal{L}_{\text{Dagger}}(B, \theta)$
- 8: **end for**

At each timestep t , the agent updates its hidden state s_t and predicts an action distribution p_t^a :

$$s_t, p_t^a = \text{HA-VLN-VL}(s_{t-1}, X, V_t),$$

where X is the tokenized instruction (often referencing multiple humans or group interactions), and V_t encodes the fused RGB-depth view. A multi-layer Transformer processes these inputs, using a specialized *state token* to attend to language and visual tokens. Final action probabilities result from an average of attention weights:

$$p_t^a = \overline{\text{AveragePool}}_{s, v}^l.$$

By fine-tuning from Prevalent [20] on HA-R2R, HA-VLN-VL concentrates on the semantic interplay between social directives and the observed scene. Further architectural details appear in Appendix C.6.

HA-VLN-CMA Agent. While HA-VLN-VL excels at interpreting nuanced instructions, **HA-VLN-CMA** prioritizes *collision avoidance & real-time adaptation* in human-filled environments. Drawing on cross-modal attention (CMA) [28], it fuses textual embeddings $l = \text{BERT}(I)$ and visual features $v_t = \text{ResNet}(o_t)$ each timestep. A multi-head attention mechanism produces a combined representation f_t , which an MLP maps to:

$$P(a_t | f_t) = \text{Softmax}(\text{MLP}_{\text{action}}(f_t)).$$

Figure A7(b) outlines the pipeline, while Appendix C.7 discusses implementation details. Human-populated settings entail partial observability and unpredictable motion. To address these challenges, we leverage *Environmental Dropout (Envdrop)* [46] & *Dataset Aggregation (Dagger)* [44]. Envdrop randomly masks features in the visual-language streams, simulating occlusions by crowds or obstructing objects. Dagger maintains a replay buffer of agent states under both expert and learned policies, enabling the agent to iteratively correct prior errors. This additional training effort improves trajectory re-planning when confronted with obstacles or unexpected human movements.

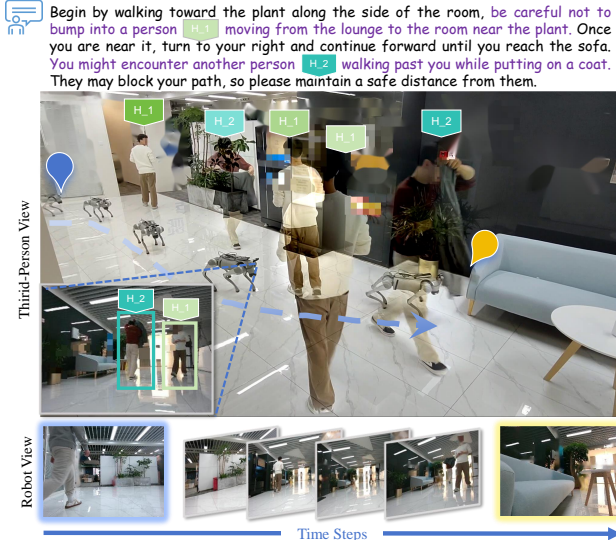


Figure 5. **Human-aware navigation with multiple bystanders.** *Top:* The robot receives instructions emphasizing caution as one person moves from the lounge to the plant while another prepares to exit. *Middle:* A third-person view highlights the robot’s trajectory and path planning among dynamic bystanders. *Bottom:* The onboard camera shows the robot’s egocentric observations.

Analysis & Insights. Figures A8 & A9 demonstrate how our agents respond to bystanders, underscoring that collision likelihood and route deviation both significantly increase when humans crowd key passageways. HA-VLN-CMA re-plans aggressively if a person suddenly blocks its immediate path, whereas HA-VLN-VL draws upon textual grounding to maintain a polite distance from social gatherings. This distinction showcases our dual innovation: a *socially enriched* dataset (HA-R2R) and specialized models that jointly facilitate robust *human-aware* navigation. Table A4 & Figure A6 further illustrate the magnitude and complexity of our annotations, emphasizing the extensive workload in data preparation, model adaptation, and thorough validation. Finally, in Section 6, we present comprehensive evaluations on *continuous* & *discrete* tasks derived from HA-R2R, illustrating the complementary strengths of HA-VLN-VL (strong language-vision fidelity) and HA-VLN-CMA (robust collision avoidance).

5. Real-World Validation & Leaderboard

Real-World Validation & Setup. We deploy our trained agents on a *Unitree Go2-EDU* quadruped, equipped with an Intel Realsense D435i RGB-D camera, MID360 3D LiDAR, and IMU for onboard perception and control. As Figure 5 illustrates, experiments are conducted in four indoor spaces (office, living room, hallway, lobby), each populated by 2–4 free-moving volunteers. The agent navigates safely in moderately congested conditions but faces challenges in

tight corridors or sudden crowd convergence, highlighting the need for robust re-planning under partial observability.

HA-R2R Test Dataset & Leaderboard. Building on R2R-CE, we present *HA-R2R*, featuring 16,844 instructions across 90 building scans with 910 annotated human models (see Sections 3 & 4). The test partition—3,408 instructions in 18 withheld buildings—intentionally emphasizes multi-human routes. While retaining path continuity from R2R-CE, we introduce refined goals to stress social awareness. The dataset is split into training (10,819), seen validation (778), unseen validation (1,839), and testing (3,408). We also host leaderboards for *HA-R2R-DE* (discrete) and *HA-R2R-CE* (continuous), focusing on both collision-related (TCR, CR) and navigation (NE, SR) metrics. Submissions may include agent code or trajectories, providing reproducible, server-side evaluations and setting a new benchmark for human-centric, dynamic VLN research.

6. Experiments

We evaluate our methods in two primary settings: (i) human-populated simulations within **HA-VLN-CE (continuous)** and **HA-VLN-DE (discrete)**, and (ii) real-world robot deployments. All evaluations use four metrics—*Navigation Error (NE)*, *Success Rate (SR)*, *Total Collision Rate (TCR)*, and *Collision Rate (CR)*—to measure navigation accuracy and social compliance. Extended formulas appear in Appendix D.1.

6.1. HA-VLN-CE: Continuous Navigation

Task Definition. HA-VLN-CE extends VLN-CE [28] by populating photorealistic 3D environments with multiple, independently moving humans. Agents navigate through continuous low-level actions based on natural-language instructions, aiming to increase **SR** while limiting collisions (**TCR**, **CR**). This setup mirrors real-world conditions where bystanders can alter their paths unexpectedly, demanding reactive policies and sophisticated sensory integration.

Baselines. We systematically benchmark two notable continuous-navigation models, BEVBert [1] and ETP-Nav [2], together with our **HA-VLN-CMA** and **HA-VLN-VL** agents. Each approach is trained/evaluated under two configurations: **Retrained**, where agents are trained/evaluated solely on HA-VLN task (HA-VLN simulator + HA-R2R instruction dataset), and **Zero-shot**, where agents are trained solely on VLN-CE task (VLN-CE simulator + R2R-CE) and evaluated on HA-VLN task.

Results. Table 1 shows pronounced gains when models incorporate HA-VLN task. For instance, BEVBert’s **SR** increases from 0.19 to 0.27 in seen split and from 0.15 to 0.21 in unseen. In stark contrast, Table 3 shows BEVBert trained on HA-VLN task performs comparably to the VLN-CE-trained one on VLN-CE task (**SR**: 0.54 vs. 0.58). This bidirectional evaluation suggests that explicit references to

Table 1. **HA-VLN-CE Results Across Validation (Seen/Unseen) and Test Splits.** “HA-VLN-CMA*” denotes the full version of HA-VLN-CMA (+DA +EV). Metrics include NE (Navigation Error, meters), TCR (Total Collision Rate), CR (Collision Rate per step), and SR (Success Rate), with lower NE/TCR/CR and higher SR indicating better performance.

Agent	Validation Seen						Validation Unseen						Test											
	Retrained			Zero-shot			Retrained			Zero-shot			Retrained			Zero-shot								
	NE↓	TCR↓	CR↓	SR↑	NE↓	TCR↓	CR↓	SR↑	NE↓	TCR↓	CR↓	SR↑	NE↓	TCR↓	CR↓	SR↑	NE↓	TCR↓	CR↓	SR↑				
HA-VLN-CMA-Base	7.63	63.09	0.77	0.05	7.88	63.84	0.75	0.04	7.34	47.06	0.77	0.07	7.95	63.96	0.76	0.03	7.30	47.55	0.76	0.07	7.89	62.14	0.74	0.04
HA-VLN-CMA-DA	6.11	17.45	0.61	0.17	6.95	37.85	0.72	0.07	7.00	27.25	0.69	0.09	7.05	38.22	0.73	0.05	7.12	28.33	0.69	0.08	6.98	36.53	0.73	0.06
HA-VLN-CMA*	5.61	3.34	0.60	0.17	7.10	29.99	0.69	0.11	6.23	8.10	0.69	0.10	6.62	32.48	0.70	0.09	6.64	9.23	0.72	0.09	7.09	31.80	0.75	0.09
HA-VLN-VL	5.02	4.44	0.52	0.20	7.82	3.67	0.45	0.05	5.35	6.63	0.59	0.14	7.15	3.97	0.46	0.06	5.52	5.96	0.63	0.14	7.41	3.38	0.58	0.07
BEVBert [1]	5.53	3.64	0.46	0.27	6.11	4.29	0.47	0.19	5.51	4.71	0.55	0.21	6.10	5.72	0.56	0.15	6.33	4.25	0.58	0.18	6.54	4.39	0.54	0.14
ETPNav [2]	5.17	4.07	0.43	0.24	7.72	6.31	0.61	0.12	5.43	6.94	0.58	0.17	7.40	7.94	0.71	0.08	5.94	5.96	0.58	0.16	7.59	5.64	0.73	0.09

Table 2. **DE Performance comparison** between agents trained/evaluated solely on VLN and agents trained/evaluated solely on HA-VLN-DE (Unseen Environments).

Agent	VLN			HA-VLN-DE		
	NE↓	SR↑	NE↓	TCR↓	CR↓	SR↑
Speaker-Follower [12]	6.62	0.35	7.44	0.32	0.72	0.21
Rec (PREVALENT) [20]	3.93	0.63	6.12	0.29	0.81	0.33
Rec (OSCAR) [20]	4.29	0.59	6.12	0.28	0.78	0.34
Airbert [16]	4.01	0.62	5.54	0.30	0.83	0.36

Table 3. **Cross-Evaluation of BEVBert (CE) vs. Rec (PREVALENT) (DE).** Each model is trained/validated under different simulators (HA-VLN-CE/HA-VLN-DE vs. VLN-CE/VLN-DE) and different instruction sets (HA-R2R vs. R2R-CE/R2R). The gray cells () indicate performance changes when models are trained on R2R/R2R-CE instructions but validated on HA-R2R.

Env	Training		Validation		Val (Unseen)	
	Simulator	Instr.	Simulator	Instr.	NE↓	SR↑
CE	VLN-CE	R2R-CE	VLN-CE	R2R-CE	4.57	0.58
		HA-R2R		R2R-CE	5.11	0.54
		HA-R2R		R2R-CE	4.35	0.27
		R2R-CE		R2R-CE	4.13	0.29
	HA-VLN-CE	HA-R2R	HA-VLN-CE	HA-R2R	5.51	0.21
		HA-R2R		HA-R2R	6.23 (↑13.1%)	0.15 (↓28.6%)
		R2R-CE		R2R-CE		
		R2R		R2R	3.93	0.63
DE	VLN-DE	R2R	VLN-DE	R2R	4.62	0.55
		R2R		R2R	5.86	0.36
		HA-R2R		R2R	5.21	0.33
		HA-R2R		HA-R2R	5.01	0.39
		R2R		HA-R2R	6.11 (↑22.0%)	0.24 (↓38.5%)

Table 4. **Impact of Human Presence (hp) and Interaction Enrichment (enrich).** We evaluate without hp (replace human with cylinders) and without enrich (skip interaction & movement enrichment in Appendix B.5) on both CE and DE settings.

hp	enrich	Env	Agent	NE↓	TCR↓	CR↓	SR↑
✓	✓	CE	BEVBert	6.10	5.72	0.56	0.15
			ETPNav	7.40	7.94	0.71	0.08
			Rec (PREVALENT)	7.31	0.31	0.79	0.22
✓	✗	CE	BEVBert	6.32 (↑3.6%)	5.11 (↓10.7%)	0.46 (↓17.9%)	0.17 (↑13.3%)
			ETPNav	7.35 (↑0.6%)	6.12 (↓22.9%)	0.63 (↓11.3%)	0.10 (↑25.0%)
			Rec (PREVALENT)	7.52 (↑2.9%)	0.27 (↓12.9%)	0.64 (↓19.0%)	0.27 (↑22.7%)
✗	✗	CE	BEVBert	6.13 (↑0.5%)	3.25 (↓43.2%)	0.35 (↓37.5%)	0.19 (↓26.7%)
			ETPNav	7.75 (↑4.7%)	4.47 (↓43.7%)	0.53 (↓25.4%)	0.14 (↓75.0%)
			Rec (PREVALENT)	7.33 (↑0.3%)	0.19 (↓38.7%)	0.42 (↓46.8%)	0.26 (↑18.2%)

dynamic crowd behavior enhance real-world navigational readiness and confirm the robustness of HA-VLN task.

Ablation Studies. (1) *Discrete vs. Continuous.* Table 2 finds that discrete agents can achieve moderate SR yet suf-

Table 5. **Impact of Step Size on Navigation.** In this experiment, the collision is detected only at the endpoint of a step, thus increasing the step size transitions from finer-grained (CE-like) control to more discrete (teleport-potential) steps. We show results for both BEVBert [1] and ETPNav [2] on seen/unseen validations. The default step size for CE is 0.25 m.

Agent	Step Size	Validation (Seen)				Validation (Unseen)			
		NE↓	TCR↓	CR↓	SR↑	NE↓	TCR↓	CR↓	SR↑
BEVBert [1]	0.10	5.65	8.43	0.50	0.23	5.41	12.60	0.54	0.22
	0.25 (CE Default)	5.53	3.64	0.46	0.27	5.51	4.71	0.55	0.21
	0.40	5.60	1.77	0.39	0.28	5.63	2.63	0.44	0.25
	1.00	5.82	0.42	0.21	0.29	5.54	0.63	0.26	0.26
ETPNav [2]	0.25	7.66	0.09	0.10	0.03	7.23	0.10	0.10	0.03
	0.50	5.15	11.70	0.54	0.20	5.47	18.66	0.64	0.16
	1.00	5.17	4.07	0.43	0.24	5.43	6.94	0.58	0.17
	2.25	5.11	2.43	0.36	0.26	5.32	3.77	0.46	0.21

fer high collisions in crowded scenes, implying simpler viewpoint-based control is inadequate for dynamic social contexts. (2) *Cross-domain Generalization.* Table 3 reveals that HA-R2R-trained agents achieve **comparable SR** to R2R-CE-trained agents (0.27 vs. 0.29) on R2R-CE validation set, while they outperform by +28.6% **SR** on the HA-R2R validation set, showcasing HA-R2R improves in-domain performance while maintaining cross-domain robustness. (3) *Human Presence and Interaction Enrichment.* Table 4 shows in human presence ablations, replacing humans with cylinders drops **TCR** by around 36% and raises **SR** by around 10%, while removing human interaction enrichment drops **TCR** by up to 22% and raises **SR** by up to 25%, confirming humans are not merely treated as generic moving obstacles during navigation. (4) *Step Size.* Tables 5 and 7 reveal a degree of complementarity between DE and CE navigation. Table 5 shows that increasing the step size (from 0.1m to 1.0m)—approximating DE-style navigation—can improve performance. However, Table 7 highlights agents fail to navigate effectively with a 1m step size (**SR** dropping close to 0) when it is treated as four 0.25m steps. This underscores that care must be taken to account for the potentially “teleport-like” movement behaviors in DE during complementarity. (5) *Sensor Modalities.* Table 6 confirms that either adding depth or RGB consistently lowers collisions and raises **SR**, reflecting the importance of 3D cues for navigating around moving bystanders. **Insights.** These findings confirm that continuous, human-

Table 6. **Ablation on RGB/Depth Inputs.** We compare **BEVBert** [1] and **ETPNav** [2] on seen/unseen validations. \checkmark denotes the sensor is enabled, while \times is disabled. Gray cells highlight performance changes (in %) upon removing/adding a modality. Best viewed in color.

Agent	RGB	Depth	Validation (Seen)				Validation (Unseen)			
			NE \downarrow	TCR \downarrow	CR \downarrow	SR \uparrow	NE \downarrow	TCR \downarrow	CR \downarrow	SR \uparrow
BEVBert [1]	\checkmark	\times	6.23 (\uparrow 12.6%)	4.55 (\uparrow 25.0%)	0.49 (\uparrow 6.5%)	0.19 (\uparrow 29.6%)	5.79 (\uparrow 5.1%)	4.97 (\uparrow 5.5%)	0.53 (\uparrow 3.6%)	0.15 (\downarrow 28.6%)
	\times	\checkmark	5.68 (\downarrow 2.7%)	3.77 (\downarrow 3.6%)	0.48 (\uparrow 4.3%)	0.25 (\downarrow 7.4%)	5.50 (\uparrow 0.2%)	4.73 (\downarrow 0.4%)	0.53 (\uparrow 3.6%)	0.20 (\downarrow 4.8%)
	\checkmark	\checkmark	5.53	3.64	0.46	0.27	5.51	4.71	0.55	0.21
ETPNav [2]	\checkmark	\times	6.14 (\uparrow 18.8%)	6.07 (\uparrow 49.1%)	0.56 (\uparrow 30.2%)	0.17 (\uparrow 29.2%)	6.38 (\uparrow 17.5%)	7.44 (\uparrow 7.2%)	0.65 (\uparrow 12.1%)	0.13 (\downarrow 23.5%)
	\times	\checkmark	4.92 (\downarrow 4.8%)	5.45 (\uparrow 33.9%)	0.55 (\uparrow 27.9%)	0.21 (\downarrow 12.5%)	5.94 (\uparrow 9.4%)	7.23 (\uparrow 4.2%)	0.65 (\uparrow 12.1%)	0.16 (\downarrow 5.9%)
	\checkmark	\checkmark	5.17	4.07	0.43	0.24	5.43	6.94	0.58	0.17

Table 7. **Impact of Step Size Combination on Navigation.** In this experiment, we treat 1m step as four 0.25m steps, and 2.25m step as nine 0.25m steps. In this case, collisions are detected every 0.25m. We show results for **BEVBert** [1] on unseen validation.

Step Size	NE \downarrow	TCR \downarrow	CR \downarrow	SR \uparrow
1.00	6.85	26.97	0.94	0.004
2.25	8.79	112.78	0.97	0.000

Table 8. **Navigation success rate across different region layouts** with (w/) and without (w/o) human presence. Each result is averaged over 30 episodes across 3 instances of each region type.

Methods	Living Room		Office		Hallway		Lobby		ALL	
	w/o	w/	w/o	w/	w/o	w/	w/o	w/	w/o	w/
HA-VLN-CMA-Base (trained on VLN-CE)	0.23	0.08	0.26	0.08	0.30	0.13	0.24	0.07	0.26	0.09
HA-VLN-VL (trained on VLN-CE)	0.38	0.11	0.38	0.10	0.47	0.17	0.38	0.10	0.40	0.12
HA-VLN-CMA-Base (trained on HA-VLN)	0.24	0.13	0.24	0.13	0.29	0.20	0.23	0.13	0.25	0.15
HA-VLN-VL (trained on HA-VLN)	0.42	0.17	0.43	0.17	0.49	0.20	0.43	0.17	0.44	0.18

aware navigation benefits from training on multi-human data, realistic instructions referencing bystander behavior, and richer sensor inputs. Failure to address these factors can lead to more collisions and lower success, highlighting multifaceted challenges of real-world social navigation.

6.2. HA-VLN-DE: Discrete Navigation.

Task Definition. HA-VLN-DE extends panoramic VLN [3] by placing multiple moving individuals in a viewpoint-based environment. Although discrete control restricts possible movements to predefined locations, it does not eliminate collisions, as bystanders may occupy a chosen viewpoint or block key transitions in narrow corridors.

Results. Table 2 compares top discrete agents on multi-human tasks. While **Airbert** achieves a moderate **SR**=0.36, it can incur a **CR** up to 0.83, illustrating persistent collision risks. Approaches that overlook human dynamics or personal space often fail when multiple bystanders converge, particularly in tight junctions or doorways. Consequently, viewpoint-based navigation alone is insufficient for robust social navigation—adaptive collision-avoidance strategies remain essential even in discrete settings.

6.3. Real-World Experiments.

Setup. We evaluate our agents in four types of everyday indoor environments (each with three instances)—*office*, *living room*, *hallway*, and *lobby*—under two conditions: (i) w/o human presence (no bystanders) and (ii) w/ human

presence (2-4 free-moving volunteers). This setup simulates realistic indoor traffic patterns and partial observability.

Observations. As illustrated in Figure 5, the robot frequently pauses or yields to avoid oncoming pedestrians. In the absence of bystanders, it navigates smoothly (Figure A11), but collisions arise in cramped corridors or when crowds converge suddenly (Figure A12). We observe similar patterns in living-room environments (Figures A13–A14) and hallways (Figure A15).

Table 8 shows the average **NSR** (Navigation Success Rate) across 30 trials in each instance. While human presence invariably lowers **NSR**, HA-VLN-VL consistently outperforms HA-VLN-CMA-Base, demonstrating stronger adaptability to dynamic motion. Also, Table 8 shows agents trained on HA-VLN achieve higher **NSR** (0.18 vs. 0.12) than VLN-CE, demonstrating HA-R2R’s sim-to-real gain under realistic conditions. Still, partial observability and abrupt group formations remain challenging, especially in narrow passages or at congested junctions. Appendix D.5 further details performance under varying crowd densities.

Insights. These experiments confirm that simulation-trained, multi-human navigation policies can indeed transfer to physical robots. However, further refinement in collision forecasting and reactive control is needed to handle unpredictable human behavior in tight indoor settings.

7. Conclusion

We propose a *Human-Aware VLN (HA-VLN)* framework unifying discrete and continuous navigation under realistic multi-human conditions. By integrating dynamic human motion, refined annotations, and high-fidelity simulators, our *HA-R2R* dataset emphasizes human-centric instructions. Experiments show social awareness, multi-human interactions, and partial observability greatly increase complexity, reducing advanced agents’ performance. Nevertheless, our approach balances safety, efficiency, and personal space. Real-world tests confirm sim-to-real transfer, while our public leaderboard standardizes evaluations. By releasing all data, simulators, agents, and tools, we promote socially responsible, context-aware navigation in dynamic, human-populated environments.

References

[1] Dong An, Yuankai Qi, Yangguang Li, Yan Huang, Liang Wang, Tieniu Tan, and Jing Shao. Bevbert: Multimodal map pre-training for language-guided navigation. In *Proceedings of the IEEE/CVF International Conference on Computer Vision*, pages 2737–2748, 2023. 6, 7, 8, 23, 25

[2] Dong An, Hanqing Wang, Wenguan Wang, Zun Wang, Yan Huang, Keji He, and Liang Wang. Etpnav: Evolving topological planning for vision-language navigation in continuous environments. *IEEE Transactions on Pattern Analysis and Machine Intelligence*, 2024. 6, 7, 8

[3] Peter Anderson, Qi Wu, Damien Teney, Jake Bruce, Mark Johnson, Niko Sünderhauf, Ian Reid, Stephen Gould, and Anton Van Den Hengel. Vision-and-language navigation: Interpreting visually-grounded navigation instructions in real environments. In *Proceedings of the IEEE/CVF Conference on Computer Vision and Pattern Recognition*, pages 3674–3683, 2018. 1, 8, 12

[4] Peter Anderson, Ayush Shrivastava, Joanne Truong, Arjun Majumdar, Devi Parikh, Dhruv Batra, and Stefan Lee. Sim-to-real transfer for vision-and-language navigation. In *Conference on Robot Learning*, pages 671–681, 2021. 1

[5] Valts Blukis, Dipendra Misra, Ross A Knepper, and Yoav Artzi. Mapping navigation instructions to continuous control actions with position-visitation prediction. In *Conference on Robot Learning*, pages 505–518, 2018. 12

[6] Tom Brown, Benjamin Mann, Nick Ryder, Melanie Subbiah, Jared D Kaplan, Prafulla Dhariwal, Arvind Neelakantan, Pranav Shyam, Girish Sastry, Amanda Askell, et al. Language models are few-shot learners. *Advances in Neural Information Processing Systems*, 33:1877–1901, 2020. 4

[7] Howard Chen, Alane Suhr, Dipendra Misra, Noah Snavely, and Yoav Artzi. Touchdown: Natural language navigation and spatial reasoning in visual street environments. In *Proceedings of the IEEE/CVF Conference on Computer Vision and Pattern Recognition*, pages 12538–12547, 2019. 12

[8] Shizhe Chen, Pierre-Louis Guhur, Cordelia Schmid, and Ivan Laptev. History aware multimodal transformer for vision-and-language navigation. *Advances in Neural Information Processing Systems*, 34:5834–5847, 2021. 12

[9] Abhishek Das, Samyak Datta, Georgia Gkioxari, Stefan Lee, Devi Parikh, and Dhruv Batra. Embodied question answering. In *Proceedings of the IEEE/CVF Conference on Computer Vision and Pattern Recognition*, pages 1–10, 2018. 12

[10] Jacob Devlin. Bert: Pre-training of deep bidirectional transformers for language understanding. *arXiv preprint arXiv:1810.04805*, 2018. 22

[11] Bosheng Ding, Chengwei Qin, Ruochen Zhao, Tianze Luo, Xinze Li, Guizhen Chen, Wenhan Xia, Junjie Hu, Anh Tuan Luu, and Shafiq Joty. Data augmentation using llms: Data perspectives, learning paradigms and challenges. *arXiv preprint arXiv:2403.02990*, 2024. 4, 15

[12] Daniel Fried, Ronghang Hu, Volkan Cirik, Anna Rohrbach, Jacob Andreas, Louis-Philippe Morency, Taylor Berg-Kirkpatrick, Kate Saenko, Dan Klein, and Trevor Darrell. Speaker-follower models for vision-and-language navigation. *Advances in Neural Information Processing Systems*, 31, 2018. 7

[13] Xiaofeng Gao, Qiaozi Gao, Ran Gong, Kaixiang Lin, Govind Thattai, and Gaurav S Sukhatme. Dialfred: Dialogue-enabled agents for embodied instruction following. *IEEE Robotics and Automation Letters*, 7(4):10049–10056, 2022. 12

[14] Daniel Gordon, Aniruddha Kembhavi, Mohammad Rastegari, Joseph Redmon, Dieter Fox, and Ali Farhadi. Iqa: Visual question answering in interactive environments. In *Proceedings of the IEEE/CVF Conference on Computer Vision and Pattern Recognition*, pages 4089–4098, 2018. 12

[15] Jing Gu, Eliana Stefani, Qi Wu, Jesse Thomason, and Xin Wang. Vision-and-language navigation: A survey of tasks, methods, and future directions. In *Proceedings of the 60th Annual Meeting of the Association for Computational Linguistics (Volume 1: Long Papers)*, pages 7606–7623, 2022. 1, 12

[16] Pierre-Louis Guhur, Makarand Tapaswi, Shizhe Chen, Ivan Laptev, and Cordelia Schmid. Airbert: In-domain pretraining for vision-and-language navigation. In *Proceedings of the IEEE/CVF International Conference on Computer Vision*, pages 1634–1643, 2021. 7, 12

[17] Tevet Guy, Raab Sigal, Gordon Brian, Shafir Yonatan, Cohen-Or Daniel, and H. Bermano Amit. Mdm: Human motion diffusion model. *arXiv preprint arXiv:2209.14916*, 2022. 4

[18] Weituo Hao, Chunyuan Li, Xiujun Li, Lawrence Carin, and Jianfeng Gao. Towards learning a generic agent for vision-and-language navigation via pre-training. In *Proceedings of the IEEE/CVF Conference on Computer Vision and Pattern Recognition*, pages 13137–13146, 2020. 12, 13, 22

[19] Yicong Hong, Cristian Rodriguez, Yuankai Qi, Qi Wu, and Stephen Gould. Language and visual entity relationship graph for agent navigation. *Advances in Neural Information Processing Systems*, 33:7685–7696, 2020. 12

[20] Yicong Hong, Qi Wu, Yuankai Qi, Cristian Rodriguez-Opazo, and Stephen Gould. A recurrent vision-and-language bert for navigation. In *Proceedings of the IEEE/CVF Conference on Computer Vision and Pattern Recognition*, pages 1643–1653, 2021. 5, 7, 12, 13, 22

[21] Vihan Jain, Gabriel Magalhaes, Alexander Ku, Ashish Vaswani, Eugene Ie, and Jason Baldridge. Stay on the path: Instruction fidelity in vision-and-language navigation. *arXiv preprint arXiv:1905.12255*, 2019. 12

[22] Yanli Ji, Feixiang Xu, Yang Yang, Fumin Shen, Heng Tao Shen, and Wei-Shi Zheng. A large-scale rgb-d database for arbitrary-view human action recognition. In *Proceedings of the 26th ACM international Conference on Multimedia*, pages 1510–1518, 2018. 4, 14

[23] Abhishek Kadian, Joanne Truong, Aaron Gokaslan, Alexander Clegg, Erik Wijmans, Stefan Lee, Manolis Savva, Sonia Chernova, and Dhruv Batra. Sim2real predictivity: Does evaluation in simulation predict real-world performance? *IEEE Robotics and Automation Letters*, 5(4):6670–6677, 2020. 1

[24] Michał Kempka, Marek Wydmuch, Grzegorz Runc, Jakub Toczek, and Wojciech Jaśkowski. Vizdoom: A doom-based

ai research platform for visual reinforcement learning. In *2016 IEEE Conference on Computational Intelligence and Games*, pages 1–8, 2016. 12

[25] James Kennedy and Russell Eberhart. Particle swarm optimization. In *Proceedings of ICNN'95-International Conference on Neural Networks*, pages 1942–1948, 1995. 4, 14

[26] Eric Kolve, Roozbeh Mottaghi, Winson Han, Eli VanderBilt, Luca Weihs, Alvaro Herrasti, Daniel Gordon, Yuke Zhu, Abhinav Gupta, and Ali Farhadi. Ai2-thor: An interactive 3d environment for visual ai. *arXiv preprint arXiv:1712.05474*, 2017. 12

[27] Vijay Konda and John Tsitsiklis. Actor-critic algorithms. In *Advances in Neural Information Processing Systems*. MIT Press, 1999. 5

[28] Jacob Krantz, Erik Wijmans, Arjun Majumdar, Dhruv Batra, and Stefan Lee. Beyond the nav-graph: Vision-and-language navigation in continuous environments. In *European Conference on Computer Vision*, pages 104–120, 2020. 1, 5, 6, 12, 21

[29] Alexander Ku, Peter Anderson, Roma Patel, Eugene Ie, and Jason Baldridge. Room-across-room: Multilingual vision-and-language navigation with dense spatiotemporal grounding. *arXiv preprint arXiv:2010.07954*, 2020. 12

[30] Jialu Li, Hao Tan, and Mohit Bansal. Enedit: Environment editing for vision-and-language navigation. In *Proceedings of the IEEE/CVF Conference on Computer Vision and Pattern Recognition*, pages 15407–15417, 2022. 12

[31] Minghan Li, Heng Li, Zhi-Qi Cheng, Yifei Dong, Yuxuan Zhou, Jun-Yan He, Qi Dai, Teruko Mitamura, and Alexander G Hauptmann. Human-aware vision-and-language navigation: Bridging simulation to reality with dynamic human interactions. *arXiv preprint arXiv:2406.19236*, 2024. 1, 2, 3, 4, 12, 14

[32] Xiuju Li, Xi Yin, Chunyuan Li, Xiaowei Hu, Pengchuan Zhang, Lei Zhang, Lijuan Wang, Houdong Hu, Li Dong, Furu Wei, Yejin Choi, and Jianfeng Gao. Oscar: Object-semantics aligned pre-training for vision-language tasks. *European Conference on Computer Vision*, 2020. 13

[33] Kunyang Lin, Peihao Chen, Diwei Huang, Thomas H Li, Mingkui Tan, and Chuang Gan. Learning vision-and-language navigation from youtube videos. In *Proceedings of the IEEE/CVF International Conference on Computer Vision*, pages 8317–8326, 2023. 12

[34] Shilong Liu, Zhaoyang Zeng, Tianhe Ren, Feng Li, Hao Zhang, Jie Yang, Qing Jiang, Chunyuan Li, Jianwei Yang, Hang Su, et al. Grounding dino: Marrying dino with grounded pre-training for open-set object detection. In *European Conference on Computer Vision*, pages 38–55, 2024. 18

[35] Jiasen Lu, Dhruv Batra, Devi Parikh, and Stefan Lee. Vilbert: Pretraining task-agnostic visiolinguistic representations for vision-and-language tasks. *Advances in Neural Information Processing Systems*, 32, 2019. 13

[36] Chih-Yao Ma, Jiasen Lu, Zuxuan Wu, Ghassan AlRegib, Zsolt Kira, Richard Socher, and Caiming Xiong. Self-monitoring navigation agent via auxiliary progress estimation. *arXiv preprint arXiv:1901.03035*, 2019. 13

[37] Matt MacMahon, Brian Stankiewicz, and Benjamin Kuipers. Walk the talk: Connecting language, knowledge, and action in route instructions. *Def*, 2(6):4, 2006. 12

[38] Khanh Nguyen, Debadatta Dey, Chris Brockett, and Bill Dolan. Vision-based navigation with language-based assistance via imitation learning with indirect intervention. In *Proceedings of the IEEE/CVF Conference on Computer Vision and Pattern Recognition*, pages 12527–12537, 2019. 12

[39] Cosmin Paduraru, Daniel J. Mankowitz, Gabriel Dulac-Arnold, Jerry Li, Nir Levine, Sven Gowal, and Todd Hester. Challenges of real-world reinforcement learning:definitions, benchmarks & analysis. *Machine Learning Journal*, 2021. 1

[40] Mathis Petrovich, Michael J Black, and Gürkaynak Varol. Action-conditioned 3d human motion synthesis with transformer vae. In *Proceedings of the IEEE/CVF International Conference on Computer Vision*, pages 10985–10995, 2021. 4, 14

[41] Xavier Puig, Eric Undersander, Andrew Szot, Mikael Dalaire Cote, Tsung-Yen Yang, Ruslan Partsey, Ruta Desai, Alexander William Clegg, Michal Hlavac, So Yeon Min, et al. Habitat 3.0: A co-habitat for humans, avatars and robots. *arXiv preprint arXiv:2310.13724*, 2023. 12, 13

[42] Xavier Puig, Eric Undersander, Andrew Szot, Mikael Dalaire Cote, Tsung-Yen Yang, Ruslan Partsey, Ruta Desai, Alexander Clegg, Michal Hlavac, So Yeon Min, Vladimír Vondruš, Theophile Gervet, Vincent-Pierre Berges, John M Turner, Oleksandr Maksymets, Zsolt Kira, Mrinal Kalakrishnan, Jitendra Malik, Devendra Singh Chaplot, Unnat Jain, Dhruv Batra, Akshara Rai, and Roozbeh Mottaghi. Habitat 3.0: A co-habitat for humans, avatars, and robots. In *Proceedings of the Twelfth International Conference on Learning Representations*, 2024. 3

[43] Yuankai Qi, Qi Wu, Peter Anderson, Xin Wang, William Yang Wang, Chunhua Shen, and Anton van den Hengel. Reverie: Remote embodied visual referring expression in real indoor environments. In *Proceedings of the IEEE/CVF Conference on Computer Vision and Pattern Recognition*, pages 9982–9991, 2020. 12, 13

[44] Stéphane Ross, Geoffrey Gordon, and Drew Bagnell. A reduction of imitation learning and structured prediction to no-regret online learning. In *Proceedings of the fourteenth international conference on artificial intelligence and statistics*, pages 627–635, 2011. 5

[45] Manolis Savva, Abhishek Kadian, Oleksandr Maksymets, Yili Zhao, Erik Wijmans, Bhavana Jain, Julian Straub, Jia Liu, Vladlen Koltun, Jitendra Malik, et al. Habitat: A platform for embodied ai research. In *Proceedings of the IEEE/CVF International Conference on Computer Vision*, pages 9339–9347, 2019. 4, 12, 13

[46] Hao Tan, Licheng Yu, and Mohit Bansal. Learning to navigate unseen environments: Back translation with environmental dropout. *arXiv preprint arXiv:1904.04195*, 2019. 5, 12, 13

[47] Jesse Thomason, Michael Murray, Maya Cakmak, and Luke Zettlemoyer. Vision-and-dialog navigation. In *Conference on Robot Learning*, pages 394–406, 2020. 12

[48] An Vuong, Toan Nguyen, Minh Nhat Vu, Baoru Huang, HTT Binh, Thieu Vo, and Anh Nguyen. Habicrowd: A high

performance simulator for crowd-aware visual navigation. In *2024 IEEE/RSJ International Conference on Intelligent Robots and Systems*, pages 5821–5827, 2024. 3, 12, 13

[49] Hanqing Wang, Wei Liang, Luc Van Gool, and Wenguan Wang. Towards versatile embodied navigation, 2022. 1

[50] Xin Wang, Qiuyuan Huang, Asli Celikyilmaz, Jianfeng Gao, Dinghan Shen, Yuan-Fang Wang, William Yang Wang, and Lei Zhang. Reinforced cross-modal matching and self-supervised imitation learning for vision-language navigation. In *Proceedings of the IEEE/CVF Conference on Computer Vision and Pattern Recognition*, pages 6629–6638, 2019. 13

[51] Zun Wang, Jialu Li, Yicong Hong, Yi Wang, Qi Wu, Mohit Bansal, Stephen Gould, Hao Tan, and Yu Qiao. Scaling data generation in vision-and-language navigation. In *Proceedings of the IEEE/CVF International Conference on Computer Vision*, pages 12009–12020, 2023. 12

[52] Yi Wu, Yuxin Wu, Georgia Gkioxari, and Yuandong Tian. Building generalizable agents with a realistic and rich 3d environment. *arXiv preprint arXiv:1801.02209*, 2018. 12

[53] Fei Xia, Amir R Zamir, Zhiyang He, Alexander Sax, Jitendra Malik, and Silvio Savarese. Gibson env: Real-world perception for embodied agents. In *Proceedings of the IEEE/CVF Conference on Computer Vision and Pattern Recognition*, pages 9068–9079, 2018. 12, 21

[54] Albert Yu, Adeline Foote, Raymond Mooney, and Roberto Martín-Martín. Natural language can help bridge the sim2real gap. *arXiv preprint arXiv:2405.10020*, 2024. 1

[55] Jiazhao Zhang, Kunyu Wang, Rongtao Xu, Gengze Zhou, Yicong Hong, Xiaomeng Fang, Qi Wu, Zhizheng Zhang, and Wang He. Navid: Video-based vlm plans the next step for vision-and-language navigation. *arXiv preprint arXiv:2402.15852*, 2024. 12, 13

[56] Yue Zhang, Ziqiao Ma, Jialu Li, Yanyuan Qiao, Zun Wang, Joyce Chai, Qi Wu, Mohit Bansal, and Parisa Kordjamshidi. Vision-and-language navigation today and tomorrow: A survey in the era of foundation models. *arXiv preprint arXiv:2407.07035*, 2024. 1

[57] Gengze Zhou, Yicong Hong, and Qi Wu. Navgpt: Explicit reasoning in vision-and-language navigation with large language models. In *Proceedings of the AAAI Conference on Artificial Intelligence*, pages 7641–7649, 2024. 12, 13

[58] Fengda Zhu, Yi Zhu, Xiaojun Chang, and Xiaodan Liang. Vision-language navigation with self-supervised auxiliary reasoning tasks. In *Proceedings of the IEEE/CVF Conference on Computer Vision and Pattern Recognition*, pages 10012–10022, 2020. 12

Appendix

This supplementary material provides expanded details and results that complement the main paper. Section A offers a comprehensive literature survey focusing on three key research challenges. Section B describes our dataset construction, annotation protocols, real-time rendering methods, API design, and additional insights on annotation data. Section C presents an in-depth overview of the HA-R2R dataset and the proposed navigation agents. Finally, Section D includes detailed evaluation metrics, additional numerical results, visualized navigation outcomes, and real-world robot validation studies, each supplemented with thorough analysis. For further resources, the project page is accessible at <https://ha-vln-project.vercel.app/>, and the datasets are provided at [DATASETS](#).

A. Related Work

This appendix surveys the evolution of Vision-and-Language Navigation (VLN) tasks, simulators, and agent designs, with particular attention to how *Human-Aware VLN* (HA-VLN) advances the state of the art. We focus on three key aspects deemed critical for bridging the Sim2Real gap: (1) *Socially Compliant Navigation*, (2) *Human-Aligned Instructions and Visual Cues*, and (3) *Dynamic Environments with Human Activities and Interactions*. Table A1 summarizes how prior work compares under these dimensions.

A.1. Development of VLN Tasks

Early VLN tasks focused on basic indoor navigation—exemplified by Room-to-Room (R2R) [3, 15, 29]—and outdoor tasks like TOUCHDOWN [7] and MARCO [37]. Later efforts such as REVERIE [43] and VNLA [38] introduced object-centric or goal-driven navigation. While these approaches expanded the range

of tasks, they typically overlooked real human behavior and social contexts. Dialogue-based tasks (e.g., DialFRED [13], CVDN [47]) incorporated interactive elements but did not account for dynamically moving bystanders or social-distance constraints. Initiatives like VLN-CE [28] moved closer to real-world conditions by enabling continuous (free-motion) navigation, yet remained largely devoid of explicit human factors [21, 29, 38, 47]. HA3D [31] addressed human motion and included human-oriented instructions but did not require agents to conform to social norms—e.g., maintaining safe distances or refraining from disturbing ongoing activities. Our proposed HA-VLN addresses these gaps by embedding all three essential elements—*socially compliant navigation, human-referenced instructions, and dynamic human activities*—into a single framework. Agents must plan routes among unpredictable bystanders, interpret language mentioning people and their behaviors, and uphold social standards. This integrated setup results in a benchmark that more closely aligns with real-world navigation demands.

A.2. Simulators for VLN Tasks

A reliable simulator is essential for developing and evaluating VLN agents. Early simulators like Matterport3D [3] and House3D [52] offered photorealistic or synthetic indoor environments but lacked mobile humans. Others, such as AI2-THOR [26] and Gibson [53], introduced more interactive elements yet typically assumed static or purely synthetic contexts, thus limiting their applicability for studying social compliance. Google Street View, used in some outdoor navigation tasks, presents static imagery with occasional humans in the scene but lacks dynamic or interactive elements. HA3D [31] moved a step further by including human activities and instructions referencing people, though it did not mandate socially compliant navigation. HabiCrowd [48] integrated crowds into photorealistic domains, improving visual diversity but omitting

Table A1. Comparison of VLN tasks, simulators, and agents based on (1) *Socially Compliant Navigation*, (2) *Human-aligned Instructions and Visual Cues*, and (3) *Dynamic Environments with Human Activities/Interactions*.

	Socially Compliant Navigation	Human-aligned Instructions and Visual Cues	Dynamic Environments	Prior Work
Tasks	✗	✗	✗	MARCO [37], DRIF [5], VLN-R2R [3], TOUCHDOWN [7], REVERIE [43], DialFRED [13]
	✗	✗	✓	VNLA [38], CVDN [47], R4R [21], RxR [29], EQA [9], IQA [14]
	✗	✓	✓	VLN-CE [28]
	✓	✓	✓	HA3D [31]
Simulators	✗	✗	✗	HA-VLN (Ours)
	✗	✗	✓	Matterport3D [3], House3D [52], AI2-THOR [26], Gibson GAN [53]
	✗	✓	✓	Habitat [45], Google Street, ViZDoom [24]
	✓	✓	✓	HA3D [31]
Agents	✗	✗	✗	HA-VLN (Ours), Habitat3.0 [41]
	✓	✗	✓	EnvDrop [46], AuxRN [58], PREVALENT [18], RelGraph [19], HAMT [8]
	✓	✓	✓	Rec-VLNBERT [20], EnvEdit [30], Airbert [16], Lily [33], ScaleVLN [51]
HA-VLN Agent (Ours)	✓	✗	✓	NavGPT [57], NaVid [55], Student Force [3]
	✓	✓	✓	HA-VLN Agent (Ours)

Table A2. **Comparison with Habitat 3.0 and HabiCrowd.** Our environment extends beyond existing simulators by offering a larger variety of natural motion types, an increased number of scenario types, and explicit instruction alignment for human-aware navigation. “Num Scenes” and “Scenario Types” refer to the total annotated scans and the distinct activities or region annotations, respectively; “Natural Motions” indicates whether human motions are photorealistically rendered and not purely script-based; “Scene & Interaction” denotes whether dynamic multi-human interactions are included in the environment.

Simulator	Habitat Series	Num Scenes	Scenario Types	Natural Motions	Motion Type	Scene & Interaction	Instr. Align
Habitat 3.0 [41]	3	59	59	Yes	2	Yes	No
HabiCrowd [48]	2	480	–	No	None	No	No
Ours	1	675	90	Yes	122	Yes	Yes

human-aligned instructions. Similarly, Habitat 3.0 [45] provides high-performance simulation without extensive multi-human or social-compliance features.

By contrast, our *HA-VLN Simulator* unifies dynamic human activities, photorealistic rendering, and social-compliance requirements. Agents perceive and react to evolving bystander behaviors—such as avoiding collisions or maintaining personal space—using both discrete (panoramic) and continuous (free-motion) navigation. As shown in Table A2, HA-VLN surpasses prior simulators in terms of scene count, motion diversity, and instruction alignment, providing a comprehensive platform for training and testing socially aware VLN agents. Specifically, we introduce 675 scenes (across 90 scenarios), 122 motion types, and a cohesive framework that supports instruction-driven dynamic human interactions. By supporting both discrete and continuous action spaces, HA-VLN further broadens its potential for addressing diverse navigation goals and real-world deployment challenges.

A.3. Agents for VLN Tasks

From early attention-based and reinforcement-learning approaches [36, 43, 50] to modern vision-language pre-training [18, 32, 35], VLN agents have grown increasingly adept at parsing instructions and navigating complex environments. However, most existing solutions—including EnvDrop [46], PREVALENT [18], and VLN-BERT [20]—rely on panoramic navigation, streamlining the action space but limiting realism of their movement. Recent efforts like NavGPT [57] and NaVid [55] explore continuous, egocentric navigation in partially dynamic worlds, yet they still lack explicit attention to *human-aligned* instructions or *social compliance*. In particular, these agents may not recognize the need to maintain safe distances, avoid disturbing activities, or adapt routes with active bystanders. Our *HA-VLN* agents address these gaps by navigating among multiple, moving humans and adhering to social norms. They interpret fine-grained, human-centric instructions and leverage visual cues that reflect real-world interactions, ensuring collision-free, respectful travel. This fusion of social compliance and dynamic human contexts sets HA-VLN apart, aligning agent behavior more closely with authentic, real-world challenges.

B. Simulator Details

B.1. HAPS Dataset 2.0

We develop HAPS 2.0 to address the shortcomings of its predecessor, particularly in terms of mismatches between textual descriptions and motion data, as well as the limited diversity of region–motion associations.

Motion–Description Alignment. The original HAPS dataset contains 435 motion categories, each defined by a region (e.g., *hallway*) and a textual description (e.g., “Someone talking on the phone while pacing”). However, more than half of these pairs do not match accurately. We therefore conduct a two-round manual verification, where multiple volunteers determine whether each pair is valid. Motions that fail both rounds are removed, yielding 172 precisely aligned motions.

Diversifying Region–Motion Relationships. In the initial dataset, each region was tied to only a few rigidly defined motions (e.g., *hallway* mostly involves “pacing on a phone,” *stairs* focuses on “sliding down a banister” or “decorating the stairway”). Such narrow mappings cause biases and limit the realism of agent navigation. To remedy this, we reorganize region–motion associations, adapting the same motion to fit various environments, including both indoor and outdoor scenes. For instance, “talking on the phone” is re-contextualized to reflect whether someone is pacing upstairs or moving around a meeting room. This broader approach offers more faithful representations of human behavior and reduces environmental biases, thus improving real-world applicability.

HAPS 2.0 vs. HAPS 1.0. Table A3 quantitatively contrasts HAPS 2.0 with HAPS 1.0. We recruit 26 volunteers to evaluate every motion in both datasets on two 1–10 scales (*motion accuracy*, *motion–environment compatibility*). A motion is deemed a failure if it scores under 3 in either category or below 5 in both. As shown, HAPS 2.0 achieves higher accuracy (8.5 vs. 6.3), better compatibility (8.1 vs. 5.9), and zero failures (0 vs. 120). It also increases motion diversity (486 vs. 435) and overall annotation effort (430+ vs. 320 hours). Moreover, HAPS 2.0 refines annotation workflows and simulator design for enhanced generalization.

Altogether, HAPS 2.0 includes 26 distinct regions across 90 architectural scenes, covering 486 human activities in

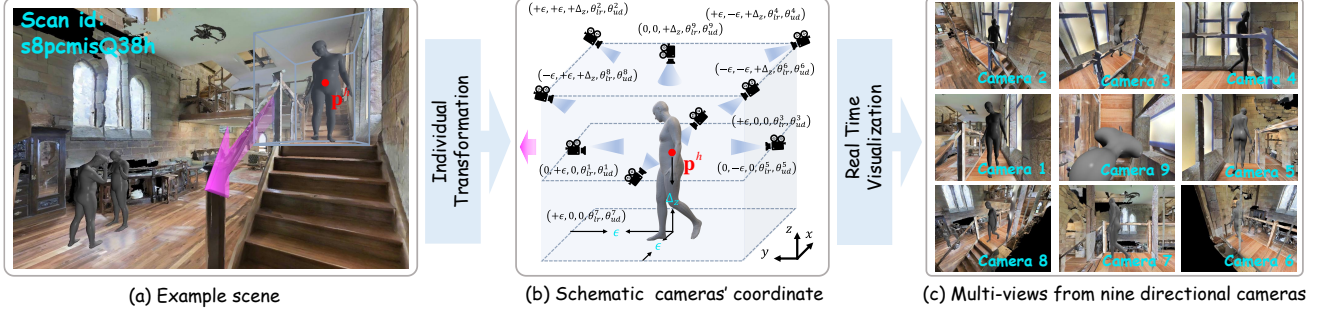


Figure A1. Multi-View Camera Setup. (a) A sample scene overview. (b) Schematic illustrating the nine camera placements around the human figure, noting key coordinates and rotations. (c) Example snapshots from the nine directional cameras, each providing a distinct viewpoint for accurate motion annotation.

both indoor and outdoor contexts. Figure A2 illustrates these improvements. By offering more accurate, flexible, and diverse depictions of human actions, HAPS 2.0 provides a robust foundation for research in human motion analysis, social navigation, and beyond.

B.2. Coarse Annotation Using PSO

We adopt a coarse-to-fine strategy for positioning human motions in 3D scans. Initially, we define each region by boundary coordinates $B_{lo} = (x_{lo}, y_{lo}, z_{lo})$, $B_{hi} = (x_{hi}, y_{hi}, z_{hi})$, and compile an object list $\mathbf{O} = \{j_1, j_2, \dots, j_n\}$ with positions \mathbf{p}^{j_i} . We then use Particle Swarm Optimization (PSO) [25] (Algorithm A1) to locate each motion h_i at an optimal position \mathbf{p}^{opt} .

Safe Distance Constraint. We set $\epsilon = 1$ m as the minimum clearance between humans and objects, ensuring a realistic layout while leaving space for agent passage.

Adaptive Penalties. Our fitness function applies penalties to placements that violate constraints (e.g., intersecting walls or overlapping humans). This strategy discourages infeasible poses and promotes plausible scene geometry alignments. The resulting coarse alignment establishes a starting point, after which we apply finer manual or semi-automated adjustments to refine multi-human interactions and ensure consistent coverage of diverse motion types.

B.3. Fine Annotation Using a Multi-Camera Setup

To refine the coarse placements of human motions, we draw inspiration from 3D skeleton-capture methods [22, 40] and deploy nine RGB cameras, each positioned around the motion site. As shown in Figure A1, this arrangement provides a comprehensive multi-view perspective, revealing potential collisions or misalignments between the human figure and surrounding objects.

Figure A1 illustrates the multi-view camera setup, showing a sample scene overview, a schematic of camera placements, and real-time visualization of multi-views from nine directional cameras.

Camera Positions & Angles. For each camera i ($i = 1, 2, \dots, 8$), we set its 3D location \mathbf{p}^{cam} to shift by Δ_x , Δ_y , and Δ_z from the base position \mathbf{p}^h . Horizontal rotation θ_{lr}^i is uniformly spaced at $\frac{\pi i}{8}$, while vertical rotation θ_{ud}^i depends on whether i is odd or even:

$$\tan \theta_{ud}^i = \begin{cases} 0, & \text{if } i \text{ is odd,} \\ \frac{\Delta_z}{\sqrt{2}\epsilon}, & \text{if } i \text{ is even.} \end{cases}$$

For the ninth camera (overhead view), $\theta_{lr}^9 = 0$ and $\theta_{ud}^9 = \frac{\pi}{2}$. These settings are ideal for general views and can be further adjusted in constrained spaces (e.g., narrow closets) or scenes requiring specialized viewpoints.

B.4. Fine Annotation Protocol

We adopt the following six-step procedure to fine-tune a human's position and orientation:

1. *Initial View.* Generate an overall preview of the human figure at \mathbf{p}^h (Figure A1(a)).
2. *Multi-Camera Observations.* Collect images from the nine cameras (Figures A1(b)–(c)). Adjust camera angles or offsets as necessary, particularly in tight scenes like small bathrooms or closets.
3. *Vertical Collision Checks.* Inspect overhead Camera 9 to detect vertical overlaps (e.g., arms interpenetrating a table). If collisions exist, identify the nearest side camera to determine how best to shift the figure.
4. *Horizontal Translation.* Modify Δ_x and Δ_y accordingly—if a nearby camera (e.g., Camera 1) reveals front-facing overlaps, shift \mathbf{p}^h by adding or subtracting based on Camera 1's perspective.

Table A3. Comparison of HAPS 1.0 vs. HAPS 2.0. We show the total number of motion categories, average *accuracy* and *compatibility* scores (both on a 1–10 scale), the number of failure cases (e.g., severe motion-description mismatches), and total annotation time. HAPS 2.0 features more diverse motions, improved motion-env alignment, and reduced failures, albeit at higher annotation effort.

Datasets	Motions \uparrow	Accuracy (1-10) \uparrow	Compatibility (1-10) \uparrow	Failure Cases \downarrow	Annotation Time (hours)
HAPS 1.0 [31]	435	6.3	5.9	120	320 (verified by [31] authors)
HAPS 2.0 (ours)	486	8.5	8.1	0	430+

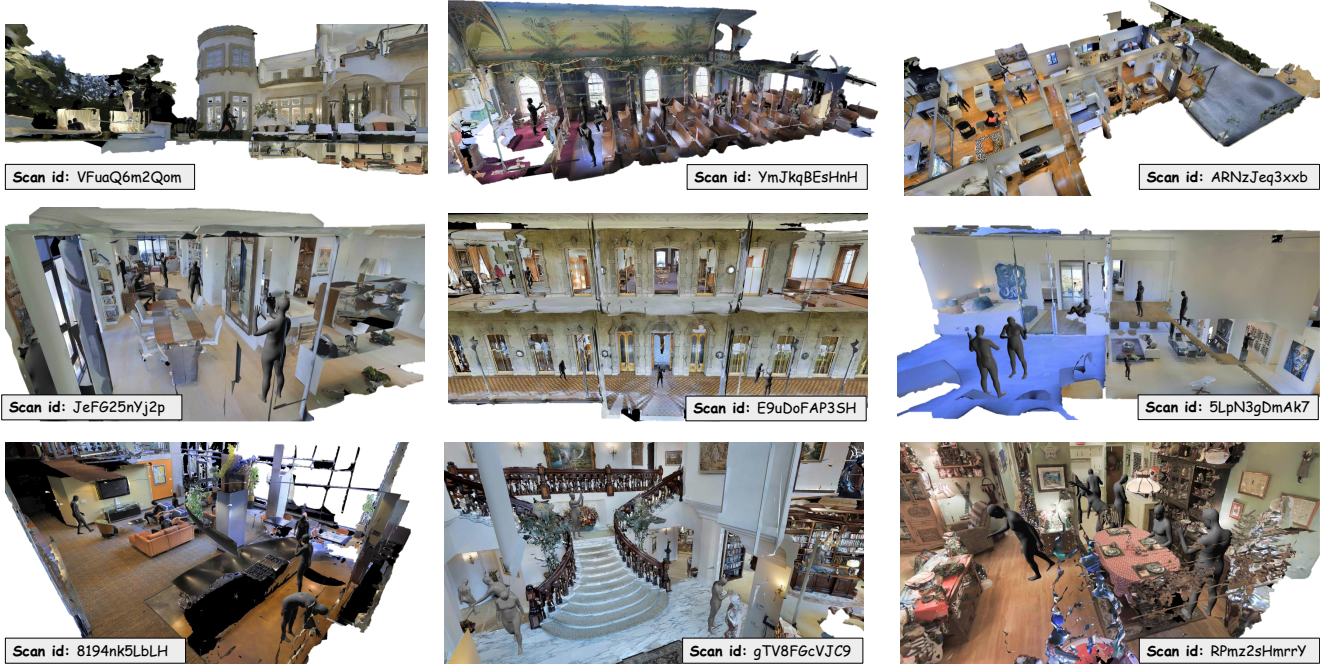


Figure A2. **Overview of HAPS 2.0 Scenes.** These examples illustrate annotated human subjects across multiple scans in the HAPS 2.0 Dataset, highlighting a range of well-aligned motions, movements, and interactions (both with objects and with other humans).

5. *Side Cameras Review.* Examine Cameras 2–8 to catch lingering overhang or collisions. Adjust the figure’s position proportionally, typically referencing a standard human height of 1.5 m to gauge whether shifts remain plausible.
6. *Finalize Output.* Upon confirming a collision-free layout, automatically generate the final video render and corresponding JSON metadata files.

This multi-camera process systematically eliminates misalignments, ensuring each human model remains properly integrated within the environment. The result is a more realistic portrayal of multi-human interactions and improved fidelity for downstream tasks.

B.5. Multi-Human Interaction & Movement Enrichment

To diversify scenes and amplify interactivity, we place additional characters into regions already featuring human motion annotations. This enables more complex interactions and varied motion trajectories. Manual insertion of extra characters, however, is time-consuming and prone to subjective bias, limiting data reliability and diversity.

Human-in-the-Loop Method. We employ large language models (LLMs) such as ChatGPT-4 and LLaMA-3-8B-Instruct to propose plausible multi-human scenarios. Each prompt integrates details about existing human motions, object positions, and regional context, guiding the LLMs to generate rich, multi-character interactions. Our prompt design uses a *system prompt* and *few-shot examples* (Listings 1

and 2) to ensure clarity and detail. For instance, we collect each human’s position and identify objects within 6 m, describing relative distances and orientations. The LLMs then construct additional human activities suited to the scene, merging them into cohesive multi-person narratives.

Iterative Annotation Workflow. After the LLMs produce candidate interactions, we merge outputs from ChatGPT-4 and LLaMA-3-8B-Instruct, then manually refine and validate them over four rounds [11]. This process corrects inconsistencies and ensures contextual alignment. We subsequently place new human motions according to the generated descriptions, leveraging our multi-camera technique (Sec. B.3) for precise annotation of complex activities (e.g., stair-walking, see Fig. A3).

Examples of Enriched Interactions. Figure 2 demonstrates how additional humans can populate a living room: “*two people sit on the couch, sharing popcorn on a small table*,” while “*a third friend stands in front of the TV, cheering*.” Such enriched scenes capture realistic multi-human behaviors—from casual gatherings to active cheering—offering agents a broader range of social cues for navigation and interaction.

B.6. Real-Time Human Rendering

We integrate dynamic human models into the simulation through a multi-threaded pipeline inspired by *Producer-Consumer* principles and Java-style signaling (check details in Algorithm A2). This setup enables agents to observe and respond to human motions in real time, facilitating adapt-



Figure A3. Movement Examples. We present representative frames from a single set of human motions, each annotated with its corresponding movement. Activities include ascending stairs, running, and pacing. For clarity, we highlight four camera views (Cameras 2, 4, 6, 8) within the multi-camera setup to provide a comprehensive perspective of human behaviors. (Zoom in for finer details.)

able navigation policies.

System Initialization. We begin by loading the environment \mathcal{E} , the set of human motions \mathbf{H} , and an object template manager \mathcal{T} that handles 3D model templates efficiently.

Signal Sender Thread (Thread 1). At intervals Δt , Thread 1 places “refresh” signals into a queue \mathcal{Q} . If \mathcal{Q} is full, it pauses until earlier signals are processed, preventing data overload. This thread models a continuous stream of human motion updates at a fixed frequency.

Main Simulation Thread (Thread 2). When the agent is about to act, Thread 2 checks \mathcal{Q} for pending refresh signals. It calculates the current frame index t as

(signals-processed mod N), where N is the total length of the human motion sequence. Template manager \mathcal{T} then removes outdated models and loads frame t into the environment, adjusting each figure’s position and orientation.

Synchronization & Consistency. We refresh human models immediately before the agent’s perception step, ensuring it observes the latest motion state. Upon starting a new episode, \mathcal{Q} is cleared, and signal counters reset, so human motions revert to frame 0, maintaining consistency across episodes. This real-time process keeps human activities synchronized with the agent’s action cycle, creating dynamically evolving scenes where agents must adapt to changing

```

"system": "You are an expert in 3D scene
understanding, specializing in generating
detailed multi-person interaction
scenarios in complex environments. I will
provide you with information about the
current human motion, object positions,
and the region context. Your task is to
infer possible additional human
interactions and describe their actions in
relation to the objects and scene."

"example": ...
//examples in Listing 2

"user": Input:
[human_motion]: "...";
[Region]: "...";
[Object_1]: "...";
[Object_2]: "...";
[Object_3]: "...";

Based on these inputs, provide a detailed,
objective description of additional people
in the scene, their locations, and their
interactions with objects and each other.
Ensure the interactions are plausible
based on the given layout and actions.

Output: ... //generation

```

Listing 1. Format of our LLM prompt for multi-human interactions & movements enrichment.

```

# Example 1
Input:
[human_motion]: "tv:An individual enjoying a sports
game, cheering loudly."
[region]: "\tv."
[TV]: "\4 meters in front of the couch, placed on a
white media console against the wall."
[couch]: "\Against the wall, 4 meters away facing
the TV."
[table]: "\1.5 meters in front of the couch,
holding some snacks and drinks."

Output:
"Three friends are gathered in the living room,
watching a movie together. Two of them are
seated comfortably on the couch, which is
positioned against the wall, facing the TV.
They are sharing popcorn and drinks placed on a
table 1.5 meters in front of the couch. The
atmosphere is relaxed, with one friend fully
focused on the movie, casually eating popcorn.
Another friend seated next to him. In front of
the TV, a third friend stands closer, about 2
meters from the couch, is more animated, loudly
cheering as they switch their attention to a
sports game playing on a different screen."

```

Listing 2. Few-shot example for for multi-human interactions & movements enrichment.

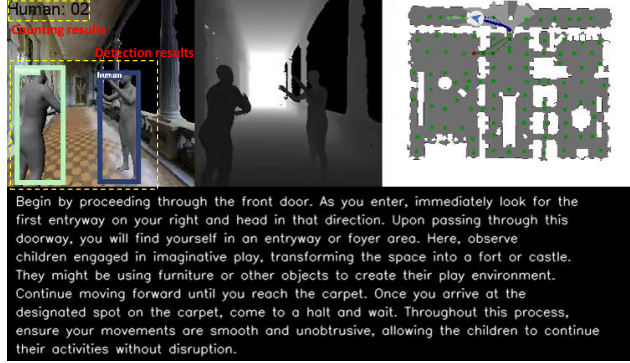


Figure A4. The visualization of Human Counting.

bystander locations and behaviors.

B.7. API Design

Discrete Environment (DE). In our discrete setting, all agent and human positions are tracked via a real-time navigational graph displayed in a 2D top-down view. Each human's activity is stored as a tuple $\langle p_h, d_{agent}, \theta_{relative}, a_{status} \rangle$, where p_h is the human's 2D coordinate, d_{agent} is the distance to the agent, $\theta_{relative}$ is the relative orientation, and a_{status} indicates the activity

state. This representation supports efficient, simultaneous tracking of multiple humans in a discrete viewpoint space.

Multi-Entity Detection & Tracking. We employ object detection on each discrete panorama to identify humans, assigning unique IDs for continuous monitoring throughout the navigation process. By linking recognized human poses to specific graph nodes, we anchor their activities to well-defined spatial references.

User Interface. A specialized UI presents a bird's-eye view of the 2D graph, allowing researchers to visualize, annotate, and adjust human behaviors in real time. This interface significantly streamlines data annotation and analysis for discrete human-aware navigation research.

Continuous Environment (CE). Our API in continuous mode mainly focuses on three components: (1) *Human Activity Monitoring*, (2) *Environmental Perception*, and (3) *Navigation Support*.

(1) Human Activity Monitoring. We track and analyze human activity in real time as in Sec. 3. When collisions occur, the agent reverts to its prior position, and we identify whether the obstacle is human or an inanimate object. For human collisions, we log the coordinates and motion state to inform potential reward-shaping strategies. Distance and orientation estimates derive from agent-human coordinate data. For instance, we employ the Grounding-

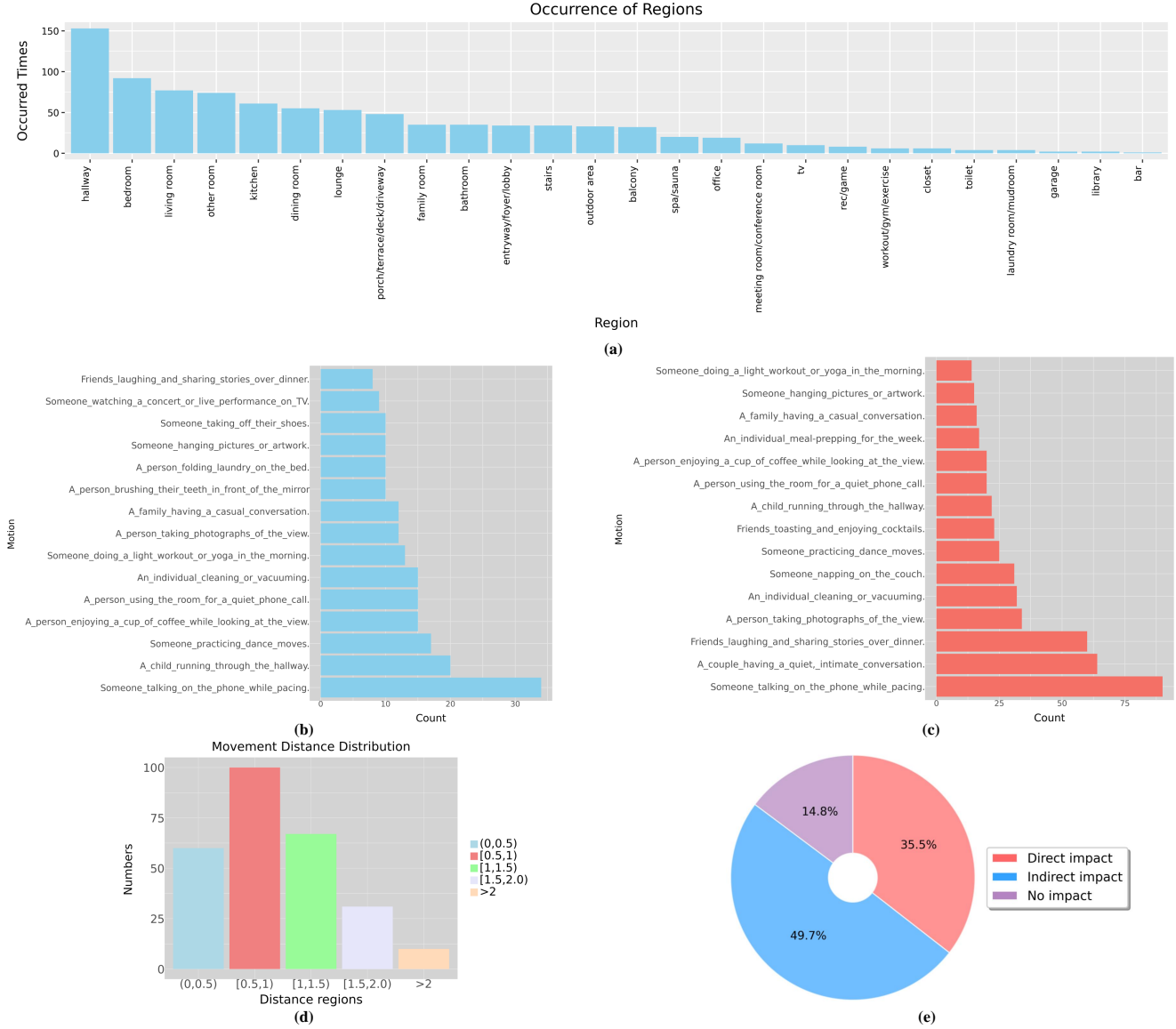


Figure A5. Statistics on human annotations in HA-VLN simulator: (a) Distribution of humans by 26 region types; (b) Top 15 motions without multi-human interaction & movement enrichment; (c) Top 15 motions with enrichment; (d) Distribution of human trajectory lengths (in meters); (e) Impact of human presence on the environment, categorized as direct, indirect, and no impact. (Zoom in to view)

DINO [34] detector on RGB inputs with the prompt “*human*” to count individuals. Figure A4 illustrates how human detection bounding boxes enable real-time counting.

(2) Environmental Perception. We maintain a dynamic scene graph comprising static elements (e.g., buildings, furniture) and moving humans. The agent continuously updates this graph by fusing positional changes and human motion data in its vicinity. This ensures real-time awareness of human activities for downstream decisions.

(3) Navigation Support. An A*-based planner computes candidate trajectories while accounting for both dynamic humans and static obstacles. During execution, we mon-

itor any divergence between the agent’s chosen route and the planner’s recommended path. This method highlights human-centric obstacles and informs the agent’s short-term re-planning steps. Our unified API supports real-time detection, tracking, and socially compliant navigation decisions in both *discrete* and *continuous* modes. It simplifies multi-human scene management, ensures intuitive collision handling, and provides robust path-planning assistance—together forming a foundation for advanced human-aware navigation algorithms.

Algorithm A1 Coarse Annotation via PSO

Require: Region $\mathbf{R} \leftarrow \langle \mathbf{r}, \mathbf{B}_{lo}, \mathbf{B}_{hi} \rangle$, where \mathbf{r} is region label and boundary coordinates $\mathbf{B}_{lo} = (x_{lo}, y_{lo}, z_{lo})$ and $\mathbf{B}_{hi} = (x_{hi}, y_{hi}, z_{hi})$; object list $\mathbf{O} \leftarrow \{j_1, j_2, \dots, j_n\}$ with positions $\mathbf{p}_{j_i} \leftarrow (x_{j_i}, y_{j_i}, z_{j_i})$; human motion set \mathbf{H} ; minimum safe distance $\epsilon \leftarrow 1$ m; height offset $\Delta_z \leftarrow 0.75$ m.

Ensure: Final positions $\mathbf{p}^h \leftarrow (x_h, y_h, z_h)$ for each human motion $h \in \mathbf{H}$.

```

1: while not all human motions placed do
2:   Filter human motions  $\mathbf{H}' \subseteq \mathbf{H}$  matching  $\mathbf{r}$ ;
3:   Match objects  $\mathbf{O}$  with human motions  $\mathbf{H}'$  based on semantic similarity to form pairs  $(h_i, j_i)$ ;
4:   for each pair  $(h_i, j_i)$  do
5:     Define search space  $\mathbf{S} \leftarrow \langle x_{lo}, x_{hi} \rangle \times \langle z_{lo}, z_{hi} \rangle \times \langle y_{lo}, y_{hi} \rangle$  around object  $j_i$ ;
6:     Initialize PSO with particles randomly positioned within  $\mathbf{S}$ ;
7:     Convergence criteria  $\leftarrow$  minimal fitness change;
8:     repeat
9:       for each particle  $p$  in the swarm do
10:        Compute position  $\mathbf{p}^h$  of particle  $p$ ;
11:        Compute fitness  $f(p)$ ;
12:         $f(p) \leftarrow d(\mathbf{p}^h, \mathbf{p}^{j_i}) + P_{\text{constraints}}(p)$ ;
13:        where  $d(\mathbf{p}^h, \mathbf{p}^{j_i})$  is the Euclidean distance, and  $P_{\text{constraints}}(p)$  is the penalty for constraint violations;
14:        Constraints:
15:         $d(\mathbf{p}^h, \mathbf{p}^{j_i}) \leq 1$  m; (Proximity to target object)
16:         $d(\mathbf{p}^h, \mathbf{p}^{j_u}) \geq \epsilon, \forall j_u \in \mathbf{O}, j_u \neq j_i$ ; (Maintain safe distance from other objects)
17:         $\mathbf{p}^h \in \mathbf{R}$ ; (Within region boundaries)
18:        Optional:  $z_h \geq z_{j_i} + \Delta_z$ ; (Height offset)
19:      end for
20:      Update particle velocities and positions using PSO update equations;
21:      until convergence criteria met
22:      Assign best particle position  $\mathbf{p}^h$  to  $h_i$ ;
23:      if no feasible solution found then
24:        Adjust PSO parameters and retry;
25:      end if
26:    end for
27:  end while

```

B.8. Human Activities Annotation Data Analysis

Human Distribution by Region. Figure A5(a) illustrates the distribution of 910 humans across 26 region types in 90 buildings, averaging about nine individuals per building. Even though each person moves independently, this distribution ensures robust and dynamic multi-human interactions, closely mirroring real-world scenarios.

Algorithm A2 Real-time Human Rendering in Simulation

Require: Simulation environment \mathcal{E} ; Human motion data \mathbf{H} ; Signal queue \mathcal{Q} with maximum size $M \leftarrow 120$; Total frames $N \leftarrow 120$; Frame interval Δt .

Ensure: Continuous real-time rendering of \mathbf{H} within \mathcal{E} .

```

1: Initialize simulator  $\mathcal{E}$ , object template manager  $\mathcal{T}$  in  $\mathcal{E}$ , human motion data  $\mathbf{H}$  and signal queue  $\mathcal{Q}$ ;
2: Initialize total signals sent and processed to 0;
3: // Thread 1: Signal sender thread
4: while true do
5:   if not  $\mathcal{Q}.\text{full}()$  then
6:     Enqueue signal “REFRESH_HUMAN” into  $\mathcal{Q}$ ;
7:     Increment total signals sent;
8:   end if
9:   Sleep for  $\Delta t$ ;
10: end while
11: // Thread 2: Main thread
12: while simulation is running do
13:   if new episode starts then
14:     Clear  $\mathcal{Q}$  and reset total signals sent to 0;
15:     Remove previous human models from  $\mathcal{E}$ ;
16:   end if
17:   // Agent handles signals before observation
18:   while not  $\mathcal{Q}.\text{empty}()$  do
19:     Dequeue signal from  $\mathcal{Q}$ ;
20:      $t \leftarrow (\text{total signals processed}) \bmod N$  {Compute current frame index};
21:     Remove previous human models from  $\mathcal{E}$ ;
22:     for each human motion  $h \in \mathbf{H}$  do
23:       Retrieve motion category, translation, and rotation of  $h$  at frame  $t$ ;
24:       Load template  $\tau_h$  into  $\mathcal{T}$ ;
25:       Add human  $o_h$  to  $\mathcal{E}$  using template  $\tau_h$ ;
26:       Set translation and rotation of  $o_h$ ;
27:     end for
28:     Increment total signals processed;
29:   end while
30:   Agent observes environment and makes decision;
31: end while

```

Motion Frequency Analysis. Figures A5(b)–(c) compare the 15 most frequent motions before and after multi-human enrichments. While the total number of motions increases, we also embed additional movement patterns and group interactions into existing actions. For instance, “*talking on the phone while pacing*” may now involve extended pacing distances or layered scenarios like “*a couple having a quiet conversation*” or “*friends sharing stories over dinner*.”

Movement Distance Analysis. Figure A5(d) displays the distribution of trajectory lengths for actively moving humans. Specifically, 22.4% cover distances up to 0.5 m, 37.3% reach 0.5–1 m, 25.0% span 1–1.5 m, 11.6% extend

Table A4. **Instruction Samples from the HA-R2R Dataset.** Text in *purple* highlights *human-related actions/movements*, while text in *blue* indicates explicit *agent-human interaction* cues. These examples illustrate how HA-R2R integrates dynamic human considerations and social awareness into navigation instructions.

1. Exit the library and turn left. As you proceed straight ahead, you will enter the bedroom, <i>where you can observe a person actively searching for a lost item, perhaps checking under the bed or inside drawers</i> . Continue moving forward, <i>ensuring you do not disturb his search</i> . As you pass by, <i>you might see a family engaged in a casual conversation on the porch or terrace, be careful not to bump into them</i> . Maintain your course until you reach the closet. Stop just outside the closet and await further instructions.
2. Begin your path on the left side of the dining room, <i>where a group of friends is gathered around a table, enjoying dinner and exchanging stories with laughter</i> . As you move across this area, <i>be cautious not to disturb their gathering</i> . The dining room features a large table and chairs. Proceed through the doorway that leads out of the dining room. Upon entering the hallway, continue straight and then make a left turn. As you walk down this corridor, you might notice framed pictures along the walls. The sound of laughter and conversation from the dining room may still be audible as you move further away. Continue down the hallway until you reach the entrance of the office. Here, <i>you will observe a person engaged in taking photographs, likely focusing on capturing the view from a window or an interesting aspect of the room</i> . Stop at this point, ensuring you are positioned at the entrance without obstructing the photographer's activity.
3. Starting in the living room, <i>you can observe an individual practicing dance moves, possibly trying out new steps</i> . As you proceed straight ahead, <i>you will pass by couches where a couple is engaged in a quiet, intimate conversation, speaking softly to maintain their privacy</i> . Continue moving forward, ensuring you navigate around any furniture or obstacles in your path. As you transition into the hallway, <i>notice another couple enjoying a date night at the bar, perhaps sharing drinks and laughter</i> . <i>Maintain a steady course without disturbing them</i> , keeping to the right side of the hallway. Upon reaching the end of your path, you will find yourself back in the living room. Here, <i>a person is checking their appearance in a hallway mirror, possibly adjusting their attire or hair</i> . Stop by the right candle mounted on the wall, ensuring you are positioned without blocking any pathways.
4. Begin by leaving the room and turning to your right. Proceed down the hallway, be careful of any human activity or objects along the way. As you continue, look for the first doorway on your right. Enter through this doorway and advance towards the shelves. Once you reach the vicinity of the shelves, come to a halt and wait there. During this movement, avoid any obstacles or disruptions in the environment.

1.5–2 m, and the remaining 3.7% exceed 2 m. This wide range reflects the diverse indoor and outdoor behaviors encompassed in the dataset.

Human Impact Analysis. As shown in Figure A5(e), humans exert a notable influence on navigation paths: 35.5% of the 16,844 paths in HA-VLN physically intersect with human motion, while 49.7% of viewpoints are indirectly affected (i.e., humans are visible along the route). These statistics underline the importance of accounting for human presence and movement trajectories when designing real-world navigation agents.

C. Agent Details

C.1. HA-R2R Instruction Examples

Table A4 illustrates four sample instructions from the *Human-Aware Room-to-Room* (HA-R2R) dataset. These examples encompass multiple scenarios: multi-human interactions (e.g., 1, 2, 3), direct agent–human encounters (e.g., 1, 2, 3), situations with four or more bystanders (e.g., 3), and paths devoid of humans (e.g., 4). Together, they demonstrate how HA-R2R challenges an agent with diverse human-aligned instructions.

C.2. HA-R2R Instruction Generation

To create enriched instructions for HA-R2R, we use ChatGPT-4o and LLaMA-3-8B-Instruct to expand upon R2R-CE's original textual data. Our strategy involves a carefully crafted few-shot prompt, combining a *system prompt* (Listing 3) and *few-shot examples* (Listing 4).

Prompt Structure. The system prompt lays out guidelines for generating instructions that emphasize social context. It encourages mentioning human activities and interactions relevant to navigation paths. Few-shot examples then illustrate the desired format, including references to human behavior (e.g., “*someone quietly making a phone call; keep your voice down as you proceed*”), positional references, and object interactions.

Iterative Refinement. In early trials, the models sometimes produced extraneous or subjective content, lacking sufficient detail on human activities. We iteratively refined the system prompt and examples, clarifying the need for neutral tone, accuracy, and contextual alignment with human-related scenarios. In each round, we analyzed model outputs, identified discrepancies, and adjusted examples to showcase more detailed, coherent, and socially aware instructions. This process guided ChatGPT-4o and LLaMA-

```

"system": "You are tasked with generating an
objective and detailed description of a path and
the related scene information based on the given
input. Focus solely on observable entities and
actions in the scene, avoiding descriptions of
smell, atmosphere, or subjective feelings. Ensure
clarity and precision in object and human
activity descriptions."

"examples": ... //examples in Listing 4

"user": Input:
[instruction_text]: "...";
[start]: "...";
[during]: "...";
[end]: "...";

Please provide an objective, step-by-step description
of the path, focusing on the objects and human
activities observed at each stage of the
navigation (beginning, during, and end). Expand
your description by including character actions,
objective descriptions of objects, and details of
the movement process. Your description should
maintain a neutral tone and avoid embellishments.
Please simulate the robot's movement along the
path, while incorporating possible connections or
interactions between the robot, objects, and
human activities.

Output: ... //generation

```

Listing 3. Format of our LLM prompt for HA-R2R instruction generation.

3-8B-Instruct toward generating instructions that fully integrate human-centric elements—such as bystander activities, relevant spatial cues, and subtle behavioral recommendations. The final HA-R2R instructions thus reflect enriched scene descriptions where agents must account for diverse, real-world nuances involving human presence.

C.3. HA-R2R Data Analysis

Word Frequency Analysis. We conduct a word frequency study on HA-R2R to gauge its capacity for representing realistic, human-centric scenarios. Figures A6(a) and (b) illustrate frequently used nouns and verbs, respectively, confirming the dataset’s focus on both spatial navigation and social interactions.

Nouns. The five most common nouns are *room*, *hallway*, *turn*, *area*, and *path*, with *room* alone appearing over 15,000 times. Other notable terms (*person*, *doorway*, *kitchen*) highlight spatial complexity and social elements such as *conversation*, *activities*, and *someone*.

Verbs. The five most frequent verbs—*is*, *continue*, *proceed*, *ensuring*, *be*—reveal an action-oriented narrative, while additional terms (*engaged*, *observe*, *notice*, *avoid*, *maintain*) underscore instructions geared toward social awareness and precise route-following.

```

# Example 1:
Input:
[instruction_text]: \"Go through the
doorway to the hall. Go down the hall
past the landing. Take the first
door on the right and stop in the
doorway. \";
[start]: \"other room:A person using the
room for a quiet phone call. \";
[during]: \"other room:A person using the
room for a quiet phone call. \";
[end]: \"hallway:An individual cleaning or
vacuuming. \";

Output:
You should start from the room. Before you
walk through the doorway into the
hallway, you will notice someone
quietly making a phone call, so please
remain quiet as you move. Then,
proceed down the hallway past the
landing. As you continue through the
corridor, you will see a responsible
cleaner using a vacuum to tidy up.
Finally, your destination is at the
end of the hallway, enter the first
door on the right and stop in the
doorway.

```

Listing 4. Few-shot examples for HA-R2R instruction generation.

Human Impact Analysis. Figure A6(c) shows that most instructions contain 20–60% human-related content, reflecting the dataset’s emphasis on people in everyday scenes.

Comparisons of word clouds in Figures A6(d) and (e) confirm that while both human-aligned and non-human segments use common navigational verbs (*walk*, *left*, *right*), instructions involving humans introduce additional social context (*couple*, *man*, *painting*). This integration of interpersonal cues elevates HA-R2R beyond simple route directives, better mirroring real-world navigation challenges in human-filled environments.

C.4. Visual and Depth Embeddings

Following VLN-CE [28], we employ parallel streams to process RGB and depth images. Each viewpoint produces a set of features from two specialized ResNet-50 models:

- **RGB Features.** Let $\{v_1^{rgb}, v_2^{rgb}, \dots, v_k^{rgb}\}$, where $v_i^{rgb} \in \mathbb{R}^{2048}$, be outputs of a ResNet-50 pretrained on ImageNet.
- **Depth Features.** Let $\{v_1^d, v_2^d, \dots, v_k^d\}$, where $v_i^d \in \mathbb{R}^{128}$, be outputs of another ResNet-50 pretrained on Gibson-4+ [53] and MP3D for point-goal navigation.

We fuse these two feature streams along with a direc-

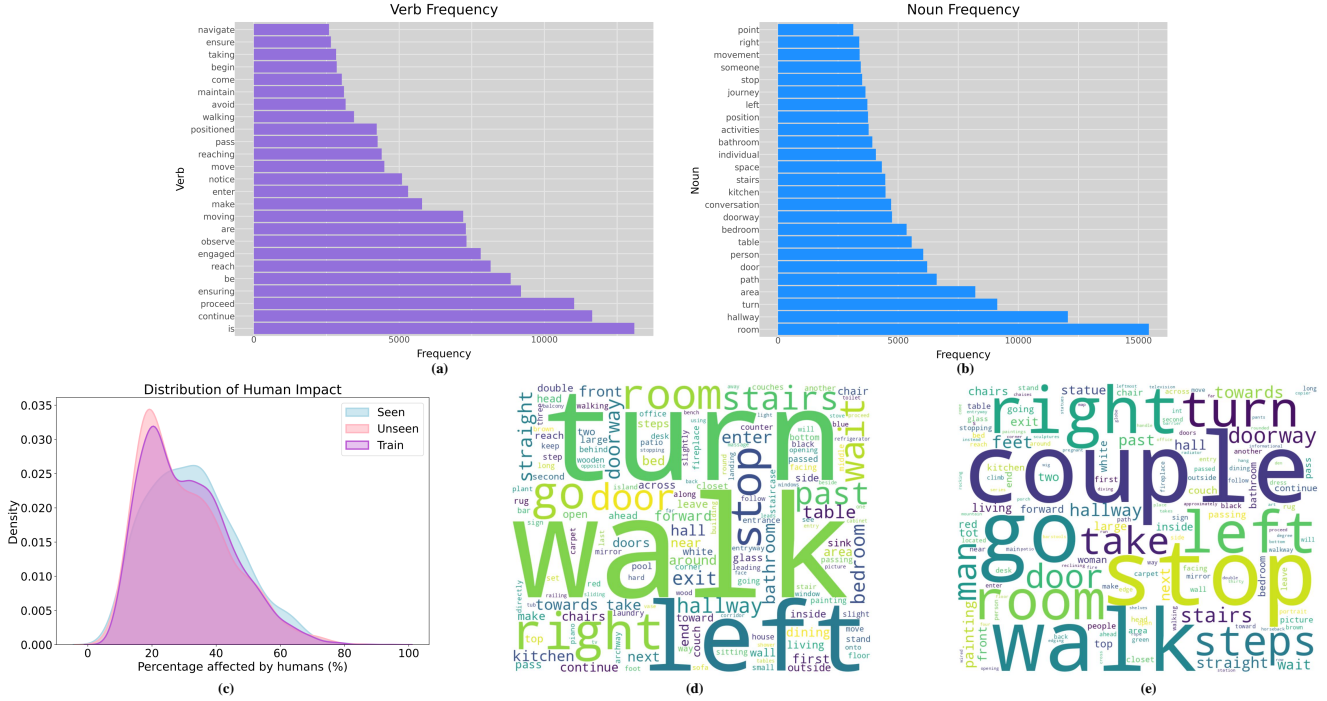


Figure A6. **Statistics for the HA-R2R Dataset.** (a) Verb frequency distribution for all instructions. (b) Noun frequency distribution for all instructions. (c) Distribution of human impact within HA-R2R (originally Fig. A4 in the main text; figure numbering differs due to inserted figures). (d) Word cloud of instructions not aligned with human activities. (e) Word cloud of instructions explicitly involving human actions. Larger font size indicates higher frequency or proportion in the dataset.

tional encoding d_i indicating spatial orientation:

$$v_i = [v_i^{rgb} W_{rgb}; \ v_i^d W_{depth}; \ d_i] W_{merge},$$

where W_{rgb} , W_{depth} , and W_{merge} are learnable projection matrices with ReLU activation. The directional encoding d_i is constructed by repeating $(\cos \theta_t^i, \sin \theta_t^i)$ 32 times, where θ_t^i measures the relative heading offset of the agent. The fused embedding $v_i \in \mathbb{R}^d$ is either 512 or 768 dimensions, matching the requirements of our **HA-VLN-CMA** or **HA-VLN-VL** agent, respectively. Both ResNet backbones remain fixed during training, ensuring consistent and stable representations from the RGB and depth channels throughout the learning process.

C.5. Text Embeddings

For the **HA-VLN-VL** agent, we utilize text embeddings from *PREVALENT* [18], which was pre-trained on 6.58M image–text–action triplets, thereby capturing broad contextual cues for navigation. Conversely, the **HA-VLN-CMA** agent adopts embeddings from *BERT* [10], also widely used for its strong language representations.

Formally, let $\ell = \{w_1, \dots, w_n\}$ be a sequence of tokens representing the instruction. Each token w_i is mapped to a one-hot vector $e_i \in \mathbb{R}^V$, where V is the vocabulary size. An embedding matrix $E \in \mathbb{R}^{V \times d}$ then projects e_i into a

continuous d -dimensional space:

$$x_i = E^\top e_i, \quad x_i \in \mathbb{R}^d.$$

In this manner, each discrete token w_i is transformed into a trainable embedding x_i , forming the foundation of the model's linguistic understanding.

C.6. HA-VLN-VL Structure

Model Overview. HA-VLN-VL adopts a BERT-like architecture inspired by Recurrent VLN-BERT [20], extending it to handle human-aware navigation. At each timestep t , the model receives the previous state s_{t-1} , language tokens X , and fused RGB-depth visual features V_t (Sec. C.4). It outputs an updated state s_t and an action distribution p_t^a :

$$s_t, \ p_t^a = \text{HA-VLN-VL}(s_{t-1}, X, V_t).$$

State Token. In line with BERT conventions, the model maintains a *state token* s_t that encapsulates the agent’s internal context. Initially, s_0 is set to the embedding of the [CLS] token. At each step, the state token is updated by appending the agent’s previously executed action a_t and projecting the resulting vector:

$$s_t = [s'_t; a_t] W_s,$$

where s'_t is the final Transformer-layer output, and W_s is a learnable projection matrix.

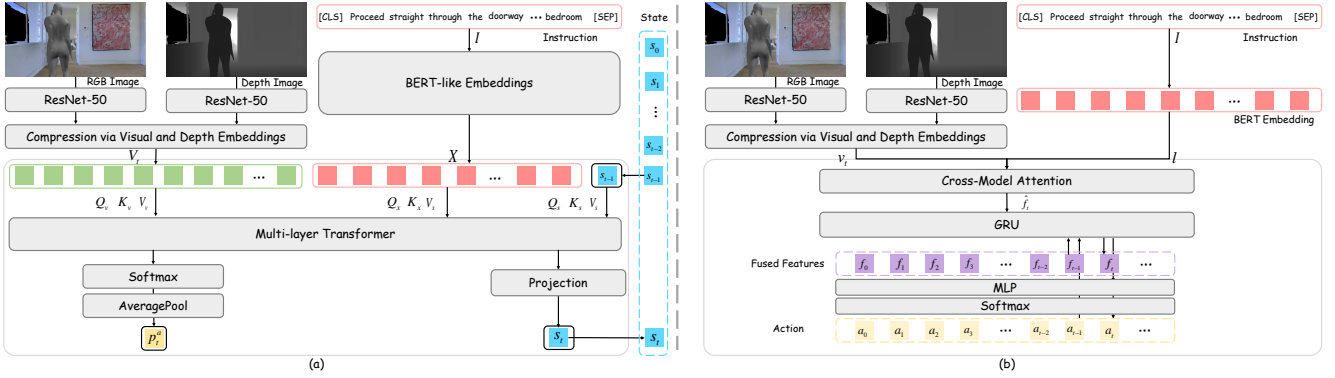


Figure A7. Network Structures. (a) **HA-VLN-VL** adopts a BERT-like transformer with a specialized state token. RGB and depth inputs are compressed by ResNet-50 and concatenated, while instruction tokens feed a BERT-like encoder. A multi-layer transformer computes cross-modal attention, producing per-step action probabilities via average-pooling and a final projection. In both architectures, continuous or discrete commands are then derived for navigation based on the agent’s policy output. (b) **HA-VLN-CMA** employs a cross-modal attention (CMA) module combined with a GRU policy. RGB and depth images are first processed by two ResNet-50 encoders and fused into a single feature stream, which attends to the instruction tokens; the fused features are then fed into a GRU and MLP to predict actions.

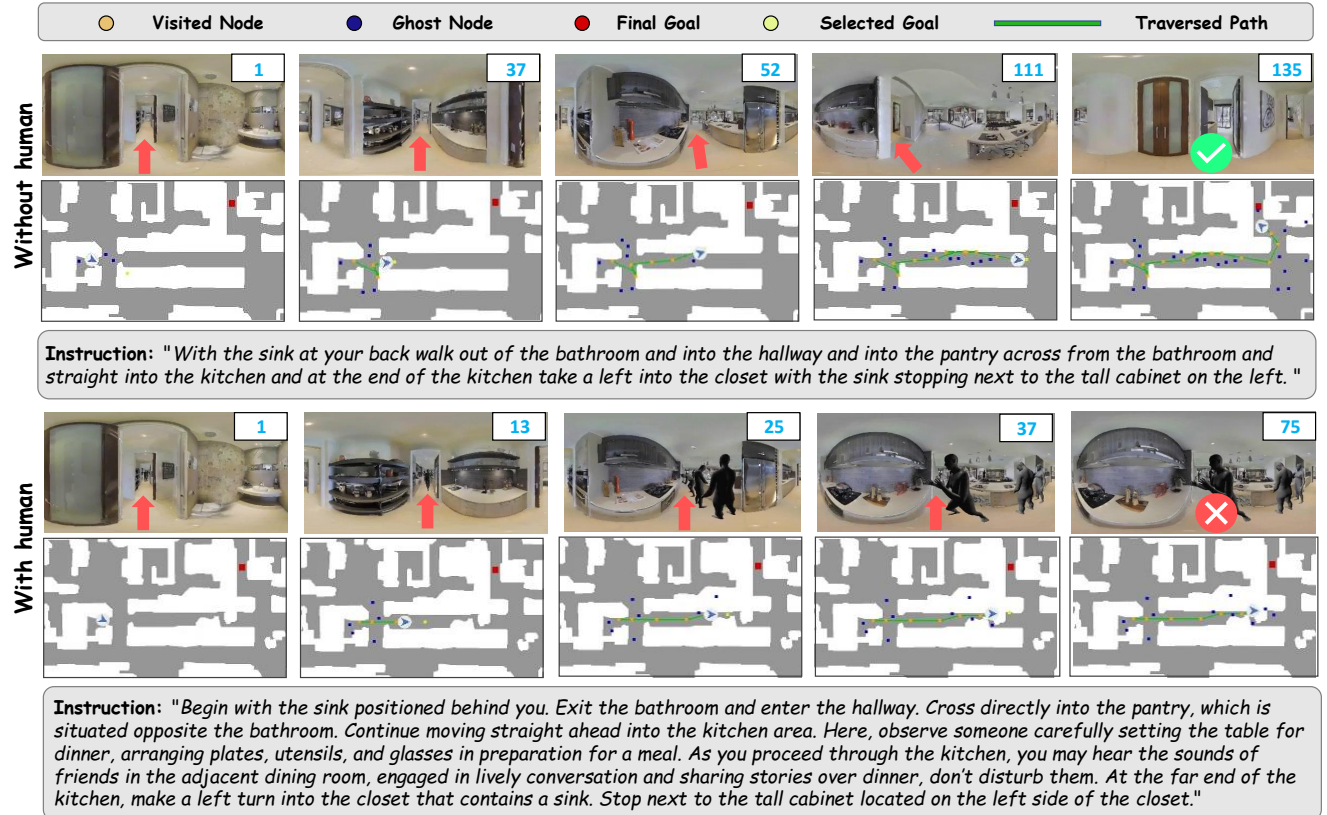


Figure A8. Trajectory Comparison Under Human vs. No-Human Conditions. We illustrate the same episode’s trajectories predicted by BEVBert [1], trained on VLN-CE, in scenarios with (bottom) and without (top) human presence. In the top row, no bystanders are present, and the agent follows its instructions with minimal collision risk. In the bottom row, bystanders and human-aligned cues lead to altered motion decisions, sometimes creating additional collision challenges or deviations.

Visual Attention. To decide the next action, we compute attention scores between s_t and the set of visual tokens $V_t = \{v_1, v_2, \dots, v_n\}$, covering navigable directions plus

a “stop” option:

$$A_{s,v}^t = \text{Softmax}\left(\frac{Q_s K_v^\top}{\sqrt{d_h}}\right),$$

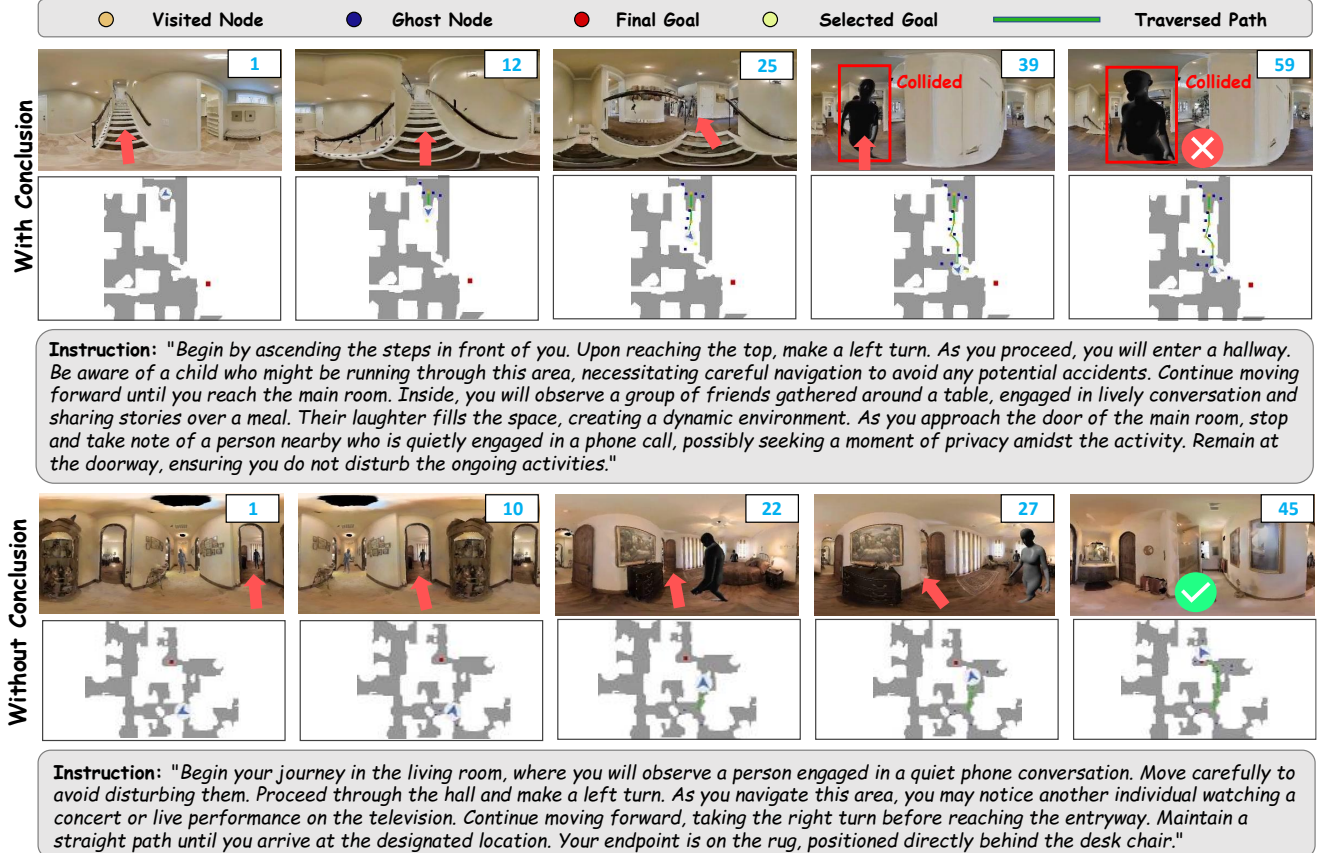


Figure A9. **Agent Trajectory Examples (HA-VLN-CMA^{*}).** The top row depicts a failed navigation case in which the agent fails to avoid an oncoming human, resulting in a collision. By contrast, the bottom row illustrates a successful run: the agent proactively adjusts its path to the right, thereby avoiding interference and completing the task collision-free.

where Q_s is derived from s_t and K_v from $v_i \in V_t$. The model then aggregates these attention scores via an average-pooling step:

$$p_t^a = \overline{\text{AveragePool}}(A_{s,v'}^t),$$

yielding an action distribution over possible moves. The agent selects:

$$a_t = \arg \max(p_t^a).$$

Training Objective. **HA-VLN-VL** is optimized through a combination of *supervised imitation learning*—to mimic ground-truth trajectories—and optional *reinforcement learning*, which rewards safe and efficient paths. As depicted in Figure A7(a), the model continuously refines its understanding of language instructions and visual cues, offering robust and socially aware navigation.

C.7. HA-VLN-CMA Structure

Architecture Overview. **HA-VLN-CMA** is a dual-stream visual-language agent featuring *Cross-Modal Attention (CMA)* and a recurrent decoder for navigation in human-populated scenarios (see Figure A7(b)). It processes two visual channels—RGB and Depth—alongside

language instructions, then outputs an action at each time step.

Dual-Stream Visual Encoding. Following Sec. C.4, each observation o_t is split into:

$$v_t^{\text{rgb}} = \text{ResNet}^{\text{rgb}}(o_t), \quad v_t^{\text{d}} = \text{ResNet}^{\text{depth}}(o_t),$$

where $\text{ResNet}^{\text{rgb}}$ and $\text{ResNet}^{\text{depth}}$ are separate backbones for RGB and Depth, respectively. The fused feature representation is

$$v_i = [v_i^{\text{rgb}} W_{\text{rgb}}; v_i^{\text{d}} W_{\text{depth}}; d_i] W_{\text{merge}},$$

where W_{rgb} , W_{depth} , and W_{merge} are projection matrices, and d_i is a direction encoding (Sec. C.4).

Language Encoder. Textual instructions $\{w_1, \dots, w_T\}$ are transformed into contextual embeddings

$$l = \text{BERT}(w_1, \dots, w_T).$$

These embeddings capture the semantic structure of the instruction and serve as input to the cross-modal module.

Cross-Modal Attention & Recurrent Decoding. At time step t , we attend to the language features using multi-head

attention:

$$\hat{f}_t = \text{MultiHeadAttn}(v_t, l),$$

where $\text{Attention}(Q, K, V) = \text{softmax}(\frac{QK^\top}{\sqrt{d_k}})V$. Multi-head attention helps handle lengthy and detailed instructions by learning multiple representations in parallel.

Next, we combine the resulting multimodal embeddings with the previous action a_{t-1} in a GRU-based decoder:

$$f_t = \text{GRU}([(v_t, l), a_{t-1}], f_{t-1}),$$

where f_{t-1} is the previous hidden state. Finally, an MLP outputs the action distribution:

$$a_t = \text{softmax}(\text{MLP}(f_t)),$$

where $\text{MLP}(f_t) = W_a f_t + b_a$, and a_t is sampled from $P(a_t|f_t)$.

Training Objectives. **HA-VLN-CMA** is trained end-to-end with a mixture of imitation learning (to mimic ground-truth paths) and reinforcement learning (to encourage collision-free, socially compliant navigation). By learning from both paradigms, the agent refines its ability to balance path efficiency and safe distancing in human-populated environments.

D. Experiments Details

D.1. Evaluation Metrics

We adopt a two-tier evaluation protocol for *HA-VLN*, measuring both *perception* (human awareness) and *navigation* (task completion). Perception metrics track how effectively the agent detects and responds to dynamic humans, while navigation metrics assess overall performance.

Total Collision Rate (TCR). Given the strong impact of human activities around critical nodes (viewpoints), we manage dynamic humans to ensure precise measurement. For navigation instance i , let A_i^c be the set of human activities at these critical nodes. We define:

$$\text{TCR} = \frac{\sum_{i=1}^L (c_i - |A_i^c|)}{L},$$

where c_i counts collisions within 1 m of a human. TCR quantifies how often collisions occur in human-occupied zones.

Collision Rate (CR). CR is the fraction of navigation instances incurring at least one collision, conditioned on the fraction β of instructions influenced by humans:

$$\text{CR} = \frac{\sum_{i=1}^L \min(c_i - |A_i^c|, 1)}{\beta L}.$$

Unlike TCR, CR highlights whether a collision occurred at all—offering insight into safety over entire trajectories.

Navigation Error (NE). NE is the mean distance between the agent’s final position and the intended target:

$$\text{NE} = \frac{\sum_{i=1}^L d_i}{L},$$

where d_i is the agent–target distance at episode end.

Success Rate (SR). SR measures the ratio of episodes completed with zero collisions:

$$\text{SR} = \frac{\sum_{i=1}^L \mathbb{I}(c_i - |A_i^c| = 0)}{L},$$

where \mathbb{I} is 1 if the agent avoids collisions, and 0 otherwise.

D.2. Ground Truth Path Annotation

In HA-VLN-CE, the agent must reach within 3 m of the target while minimizing collisions. To label ground-truth paths, we use an A*-based heuristic search that identifies the shortest viable route, dynamically re-planning when obstacles block progress.

D.3. Relative Gap of HA-VLN-CE

Table A5 reports two metrics: (1). **Retrain gap** denotes performance difference between agents trained on HA-VLN task (using HA-R2R & HA-VLN simulator) evaluated on HA-VLN task and agents trained & evaluated on VLN-CE task; (2). **Zero-shot gap** denotes the performance difference between the zero-shot HA-VLN performance of agents trained on VLN-CE task and agents trained & evaluated on VLN-CE task. Both are reported as relative percentages:

$$\text{PG} = \frac{\text{Value}_{\text{HA-VLN}} - \text{Value}_{\text{VLN-CE}}}{\text{Value}_{\text{VLN-CE}}} \times 100\%$$

The table compares agent performance on VLN-CE and the more challenging HA-VLN-CE tasks using Retrain Gap and Zero-shot Gap metrics. While retraining on HA-VLN-CE generally improves NE, all agents show a significant drop in SR. Zero-shot evaluation of VLN-CE-trained agents on HA-VLN-CE reveals substantial performance degradation across all metrics, underscoring the increased difficulty and domain shift of the HA-VLN-CE task. Besides, Table 1 shows pronounced gains when models incorporate HA-VLN task. For instance, BEVBert’s SR increases from 0.19 to 0.27 in seen split and from 0.15 to 0.21 in unseen. In stark contrast, Table 3 shows BEVBert trained on HA-VLN task performs comparably to the VLN-CE-trained one on VLN-CE task (SR: 0.54 vs. 0.58). This bidirectional evaluation suggests that explicit references to dynamic crowd behavior enhance real-world navigational readiness and confirm the robustness of HA-VLN task.

D.4. Visualization of Navigation

Figures A8 & A9 illustrate trajectories predicted by **BEVBert** [1] (trained on VLN-CE) and **HA-VLN-CMA***,

Table A5. Performance comparison in validation unseen environments on between VLN-CE task and HA-VLN-CE task. **Retrain gap** denotes performance difference between agents trained on HA-VLN task (using HA-R2R & HA-VLN simulator) evaluated on HA-VLN task and agents trained & evaluated on VLN-CE task; **Zero-shot gap** denotes the performance difference between the zero-shot HA-VLN performance of agents trained on VLN-CE task and agents trained & evaluated on VLN-CE task. († indicates HA-VLN-VL and HA-VLN-CMA employ the same model, which was trained on the VLN-CE Dataset, to achieve zero-shot performance on HA-VLN-CE.)

Agent	VLN-CE				HA-VLN-CE				Performance Gap (%)			
	VLN-CE		Retrained		Zero-shot		Retrained		Zero-shot			
	NE↓	SR↑	NE↓	SR↑	NE↓	SR↑	NE↓	SR↑	NE↓	SR↑	NE↓	SR↑
HA-VLN-CMA-Base	8.15	0.22	7.34	0.07	-	-	-9.8	-69.6	-	-	-	-
HA-VLN-CMA-DA	8.12	0.26	7.00	0.09	-	-	-13.8	-66.7	-	-	-	-
HA-VLN-CMA†	6.01	0.31	6.23	0.10	6.62†	0.09†	+3.7	-68.8	+10.2	-71.9	-	-
HA-VLN-VL	5.73	0.43	5.35	0.14	7.15†	0.06†	-6.8	-68.2	+24.6	-86.4	-	-
BEVbert	4.57	0.58	5.51	0.21	6.10	0.15	+20.6	-64.4	+33.5	-74.6	-	-
ETPNav	4.72	0.56	5.43	0.17	7.40	0.08	+15.3	-70.2	+57.1	-86.0	-	-

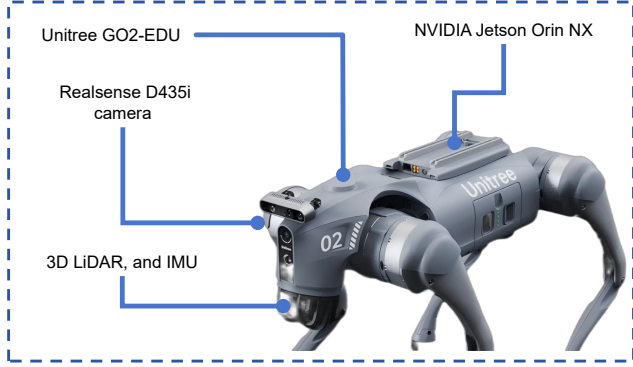


Figure A10. **Unitree GO2-EDU quadruped robot used in real-world experiments.** The platform integrates an NVIDIA Jetson Orin NX for onboard computation, an IMU for pose estimation, an Intel RealSense D435i camera for visual perception, and a 3D LiDAR for obstacle/human detection.

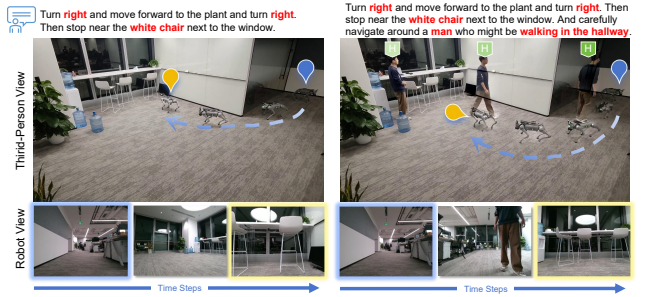


Figure A11. **Navigation success in an office setting** (left: no humans, right: with humans). **Top:** The given instruction for the robot. **Middle:** A third-person view of the robot's path. **Bottom:** The robot's egocentric camera feed.

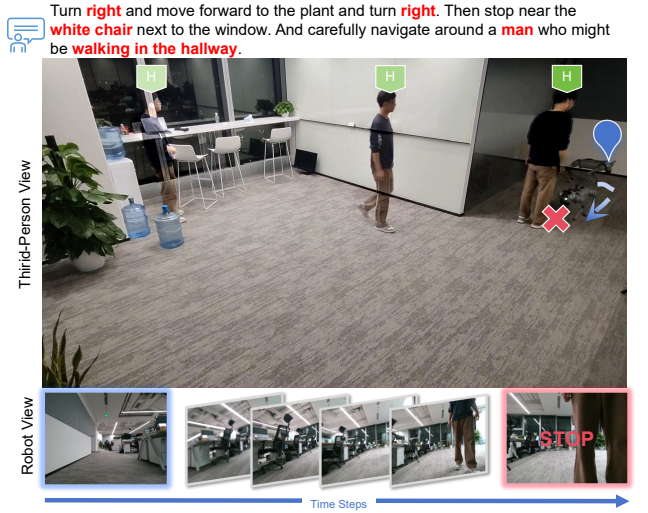


Figure A12. **Navigation failure in an office setting.** A volunteer abruptly changes position, causing the robot to collide mid-path. This scenario highlights the difficulty of adapting to sudden human movement in confined workspaces.

which showcases success and failure in human-filled or empty environments.

Failures with Human Crossing. In Figure A8, the agent performs well when no bystanders are present. Yet in a human-populated setting, it fails to adjust at step 37 when a volunteer crosses its path, leading to collision.

Collision vs. Avoidance. Figure A9 similarly shows two scenarios. At step 39 in the top pane, a direct approach by a bystander overwhelms the agent, causing a collision. In the bottom pane at step 22, the agent successfully deviates upon sensing a person nearby, avoiding any collision altogether. These visualizations confirm that dynamic human presence greatly complicates navigation, highlighting the need for robust social-aware models.

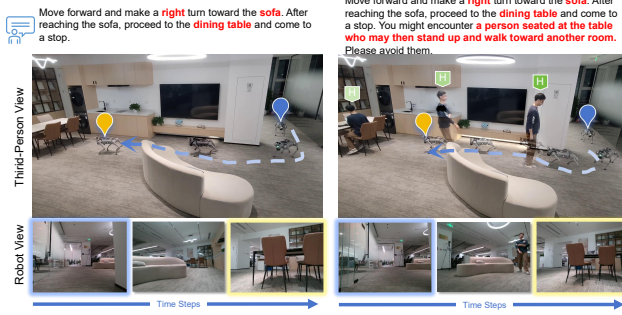


Figure A13. **Navigation success in a living room** (*left*: no bystanders, *right*: with bystanders). The robot follows instructions toward the sofa and dining area, keeping safe distances while navigating around volunteers.

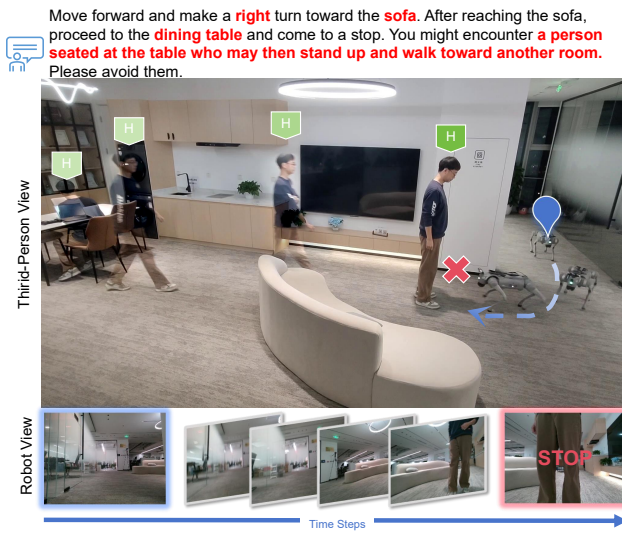


Figure A14. **Navigation failure in a living room with multiple bystanders.** Attempting to move beyond the sofa toward a dining area, the robot collides with a volunteer who abruptly stands and shifts position. This underscores how unpredictable human motion can disrupt the agent’s intended path, requiring rapid re-planning.

D.5. Validation on Real-World Robots

To deploy our navigation agents on physical hardware, the robot is equipped with an *NVIDIA Jetson NX* for AI inference and a *Raspberry Pi 4B* for motion control. The Jetson handles core navigation computations (receiving camera images and inferring action commands), while the Pi executes high-level movement directives such as *turn left* or *move forward*. We set a minimum step size of 0.25 m and a rotation increment of 15 degrees. An onboard IMU continuously monitors the robot’s orientation and position, ensuring movement commands align with issued directives.

Robot Setup. Our evaluations use a *Unitree GO2-EDU* quadruped (Figure A10), featuring an *Intel Realsense D435i* camera providing RGB imagery at 90° FOV and a 3D Li-

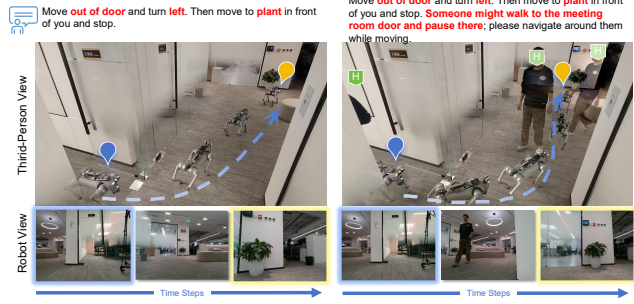


Figure A15. **Navigation success in a hallway** (*left*: no bystanders, *right*: with bystanders). When volunteers appear, the robot halts or deviates to avoid collisions, showcasing adaptive behavior in a constrained corridor.

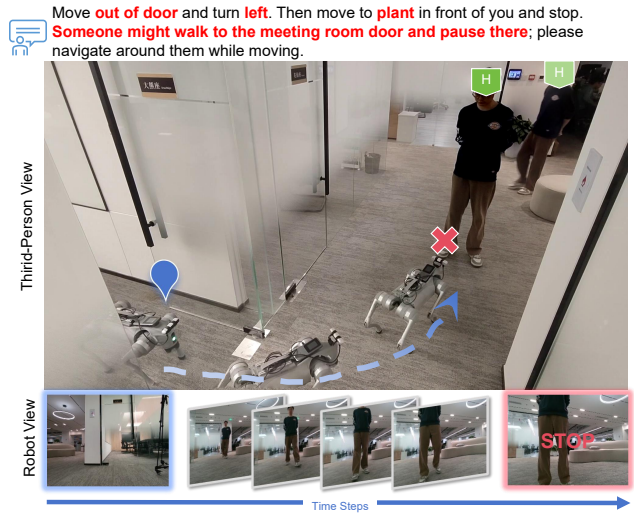


Figure A16. **Navigation failure in a hallway.** A volunteer’s sudden positional change causes a mid-path collision and mission failure, reflecting the challenge of unpredictable human movement, even in comparatively open corridors.

DAR below camera for detection. IMU refines positional and orientational control, enabling consistent motions.

Visual Demonstrations. Figures A11, A13, and A15 show the robot traversing distinct indoor environments—offices, living rooms, and hallways—guided by natural-language instructions. In Figure 5, the robot navigates around multiple people, leveraging camera inputs to avoid collisions through minor path adjustments. Although the agent typically succeeds in reaching its destination, collisions remain possible when bystanders change their trajectories unexpectedly. Figures A12, A14, and A16 illustrate such scenarios, highlighting real-time challenges in unpredictable, human-inhabited spaces. More demos including a compilation video on our project webpage, further illustrate robot’s performance and underscore how human-aware training aids sim-to-real transfer in dynamic indoor environments.